Modeling the x-ray absorption of Neodymium ions in cuprate superconductors

by

Anton Lutsenko

A thesis
presented to the University of Waterloo
in fulfillment of the
thesis requirement for the degree of
Master of Science
in
Physics

Waterloo, Ontario, Canada, 2022

Author's Declaration

I hereby declare that I am the sole author of this thesis. This is a true copy of the thesis, including any required final revisions, as accepted by my examiners.

I understand that my thesis may be made electronically available to the public.

Abstract

Electronic nematicity, a breaking of the rotational symmetry of the electronic structure beyond what is expected from the ionic displacements of atoms, has been identified in the $(\mathrm{La,M})_2\mathrm{CuO}_4$ family of the cuprate superconductors. This was achieved by measuring the temperature dependence of the (001) Bragg reflection peak intensity at resonant x-ray photon energies corresponding to different atoms within the unit cell. Recently, however, it has been identified that x-ray scattering of Nd $M_{4,5}$ edge in $(\mathrm{La,Sr,Nd})_2\mathrm{CuO}_4$ exhibits unusual increase in (001) Bragg reflection intensity when the temperature is increased from 10 to 70 K, seemingly at odds with the understanding of electronic nematicity in these systems. It was hypothesized that this change may arise from the single-ion phenomena. To test this hypothesis, polarization and temperature dependence of the x-ray absorption spectrum are analyzed. The spectrum exhibits temperature-dependent linear dichroism, which was hypothesized to be connected to the temperature dependence of the (001) scattering intensity. A numerical modeling software, Quanty, was utilized to create a two-shell model and study its properties via Monte-Carlo method. We establish that the temperature-dependent excitation into low-energy crystal field states results in significant temperature dependence to the single-ion scattering tensor. A crystalline electric field of C_{2v} symmetry with realistic parameters captures the temperature dependencies of the x-ray absorption spectrum, while also being consistent with excitation energies measured by inelastic neutron scattering. However, the calculated (001) scattering intensity decreases with temperature for all probed crystal field parameter sets, contrary to the experimentally observed increase. We speculate at future refinements to our model that may rectify this discrepancy.

Acknowledgements

I would like to thank all the people who made this thesis possible:

professor David Hawthorn, for his hospitality in the trying times,

Naman Kumar Gupta, for the guidance and responsiveness,

Mitacs, for the ultimate opportunity and financial support, and

the Armed Forces of Ukraine, for protecting the sky above me and the land around me during the completion of this thesis.

Dedication

This is dedicated to my beloved Olena, who has been together with me and supporting me through my graduate studies.

Table of Contents

List of Figures

List of Tables

List of Abbreviations

CEF crystalline electric field 24, 26, 27, 29, 31, 84

HTT high temperature tetragonal 10, 11

LTO low temperature orthorombic 10, 11, 53

LTT low temperature tetragonal 10, 11, 21, 53

TEY total electron yield 18

TFY total fluorescence yield 18

XAS x-ray absorption spectroscopy 2, 13, 14, 17, 18, 37

XMLD x-ray magnetic linear dichroism 22

XNLD x-ray natural linear dichroism 22

Chapter 1

Introduction

Cuprate superconductors were historically the first high-T_c superconductors to be discovered [1]. They have phase diagrams rich of different phases, both structural (LTT, LTO, HTT) and electronic (antiferromagnetic insulator, Fermi liquid, strange metal, charge- and spin-density wave, as well as a pseudogap phase) [2]. Understanding the connection between these phases can shine some light on the physics which regulates them and, prospectively, how the relationship of these phases can be tuned to enhance properties such as the superconducting transition temperature.

Recently, in addition to well-established phases, an electronic *nematic* phase was identified in the $(\mathrm{La,M})_2\mathrm{CuO}_4$ family of materials – a rotational symmetry breaking, distinct from structural distortions [3, 4]. It was done by measuring the (001) Bragg peak on different absorption edges in crystals of cuprate superconductors via resonant x-ray scattering. This peak is forbidden in conventional x-ray scattering. However, on resonance it is allowed because of the difference in orbital symmetry of atomic states between the neighbouring planes, and it is very sensitive to this difference. It was observed that the temperature dependencies for the planar Cu L and O K absorption edges were different from the ones for the La M or apical O K edges (Figure 1.1a) – and this discrepancy was attributed to electronic nematicity.

However, recent follow-up measurements of the temperature dependence of the (001) peak at the Nd M edge in Nd-LSCO demonstrated an anomalous temperature dependence

different from that of other constituent atoms [5], raising questions about understanding of electronic nematicity in this family of materials. Specifically, the scattering exhibits an unusual peak of intensity directly before the transition (Figure 1.1b).

The purpose of this thesis is attempt to identify the origin of the anomalous temperature dependence to the (001) peak at the Nd M edge. In order to do this, we aim to analyze the temperature and photon polarization dependence of a closely related property – x-ray absorption. The x-ray absorption coefficient is related to the atomic scattering form factor, f, which determines how strongly an x-ray scatters from an atom. Recent measurements of the x-ray absorption spectrum at Nd $M_{4,5}$ edges in Nd-LSCO demonstrates polarization and temperature dependencies [5]. Analyzing the polarization and temperature dependence of the x-ray absorption can therefore provide insight into scattering at the (001) peak. Specifically, we explore whether the thermal excitation of single-ion low-energy excited states of Nd atoms, affecting all Nd sites, contributes to the temperature dependence of the (001) peak scattering intensity

To understand the nature of the observed x-ray absorption spectrum, we utilized crystal field theory. A free Nd ion, just as any other ion, would be considered a spherically symmetrical system: there is no primary direction, and different properties (like, for example, x-ray absorption or scattering) would be the same in all directions. However, if an ion sits within a crystal, it is impacted by its neighbourhood: in some directions, its electron cloud may be attracted to or repulsed from the neighbouring charge density stronger than in other directions. This field which deforms the electron cloud is called "crystalline electric field", and is studied by crystal field theory [6, 7]. The deformed electron cloud is no longer spherically symmetric: instead, its symmetry is defined by its surrounding within the crystal. This also causes the change in a symmetry of the scattering and conductivity tensors, which is captured, correspondingly, by x-ray scattering and x-ray absorption spectroscopy.

To study the behaviour of the Nd ion within LSCO, we utilized a numerical modeling software called Quanty [8]. This software is designed for calculating various spectra, such as x-ray absorption spectroscopy (XAS), as well as expectation values, for many-electron systems. The whole ion was approximated by a smaller and simpler system, which was simulated and studied at significantly lower cost compared to the whole ion. Softwares like Quanty are especially suitable for this kind of systems.

Using this software with the crystal field theory approach, a model of the Nd^{3+} ion within Nd-doped LSCO was created. We found that the observed linear dichroism of its x-ray absorption spectrum can indeed be attributed to crystal field. This field splits the degenerate groundstate of a free Nd^{3+} ion into several states with different wavefunction symmetry, absorption spectrum, and energy. In a crystal, there is a mixture of Nd ions in different states – and the absorption spectrum of a crystal would be a mixture of single-ion spectra corresponding to these states. Realistic parameters of a crystal field with C_{2v} symmetry result in states, whose energies are consistent with the results of inelastic neutron scattering experiment, and absorption spectra – to the experimentally observed spectrum.

Despite agreement between model calculations and experiment for the x-ray absorption coefficient, we find that the temperature dependence of the (001) x-ray scattering intensity deduced from this model *differs* from the experimentally observed one. While a noted temperature depdendence is observed in our calculations associated with crystal field excited states of Nd, the resulting temperature dependence differs from experiment. We speculate at future refinements to our model calculations that may rectify the disagreement between our calculations and measurements.

This thesis is organized in a following manner. A look at the cuprates and specifically LSCO is laid out in Chapter 2. The technique of x-ray absorption spectroscopy and its connection to the properties of an ion are described in Chapter 3. The main points and relevant details of the crystal field theory are outlined in Chapter 4. The possibilities of Quanty, together with some insight into the theory behind it, are explained in Chapter 5. The detailed results of the study are presented in Chapter 6, and summarized in Chapter 7.

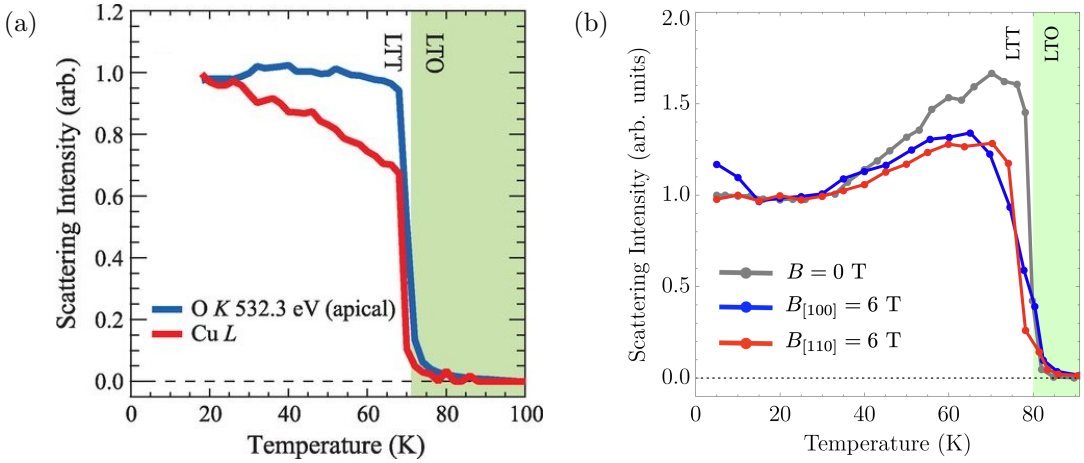

Figure 1.1: Temperature dependence of (001) Bragg peak intensities for (a) planar Cu and apical O and (b) Nd absorption edges in LNSCO crystals. When the temperature of a sample increases, the intensities of reflection peaks, measured at apical O K edge and La L edge (blue line), decrease faster then the intensities, measured at planar O K edge and Cu L edge (red line). At Nd^{3+} M edge, however, starting from $\approx 30K$ the scattering intensity increases until it reaches a peak at $\approx 70K$, and then sharply decreases to reach zero at $80K$. Adapted from [3] and [5].

Chapter 2

Cuprate superconductors

2.1 Overview

Cuprate high-temperature superconductors have been receiving a lot of attention since their discovery in 1986 [9]. Historically, the first one to be found was $La_{5-x}Ba_xCu_5O_{5(3-y)}$, with a critical temperature of 35 K at $x = 0.75$ [10]. The discovery coined a search for the materials with similar structure and higher critical temperature. In less than a year, it led to $(Y_{1-x}Ba_x)_2CuO_{4-\delta}$, with superconductivity emerging as high as 90 K at $x = 0.4$ [11].

Both of these materials, as well as their variations, are based on CuO_2 planes. These planes, under specific parameters, manifest the superconducting phase. CuO_2 planes are separated by so-called spacer layers, which act as charge reservoirs and modulate the concentration of electrons on the CuO_2 planes. There are several structural families of cuprates, each of which contains dozens of variations [12]. The structures vary in the number of spacer layers, relative positioning of copper oxide planes and spacer layers, and atomic composition and structure of spacer layers. The example structures are provided on Figure 2.1.

The LCO (or $(La, M)_2CuO_4$) family is derived from La_2CuO_4. It contains materials where the CuO_2 planes are intercalated with Lanthanum and Oxygen. Lanthanum atoms may be replaced with other atoms such as Barium, Strontium, Neodymium et cetera.

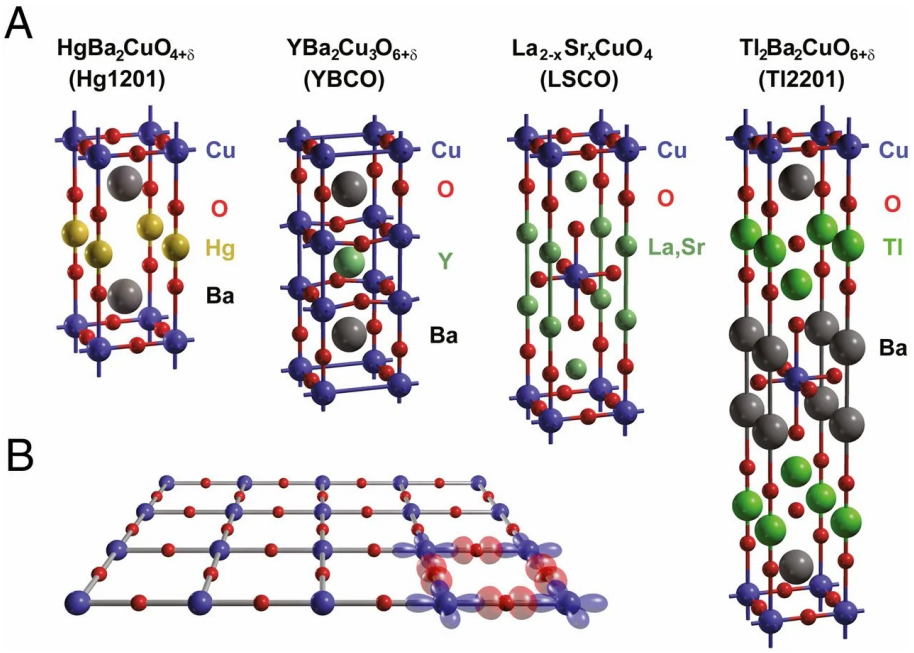

Figure 2.1: (a) The examples from the four main structure families of high-Tc superconductors: Hg-Ba-Cu-O, Y-Ba-Cu-O, La-Cu-O and Tl-Ba-Cu-O. In all of the examples, CuO squares can be noticed at the top and bottom (and sometimes in the middle) of an elementary cell. The layers between them are the spacer layers. (b) CuO_2 plane, the main structure element of cuprate superconductors. Cu $3d$ and O $2p$ orbitals, indicated on the bottom right square, are close in energy and strongly hybridized. The plane's charge density is modulated by the spacer layer atoms. Reused from [13] with permission.

Since the Ba and Sr have both a 2+ state rather than a 3+ state as La atoms are, holes are introduced into CuO_2 plane, thus significantly changing the electronic properties of the material [14]. Moreover, Oxygen stoichiometry may be increased, complementing the CuO_4 squares to make CuO_5 pyramids or CuO_6 octahedra. The example structures are provided on Figure 2.2.

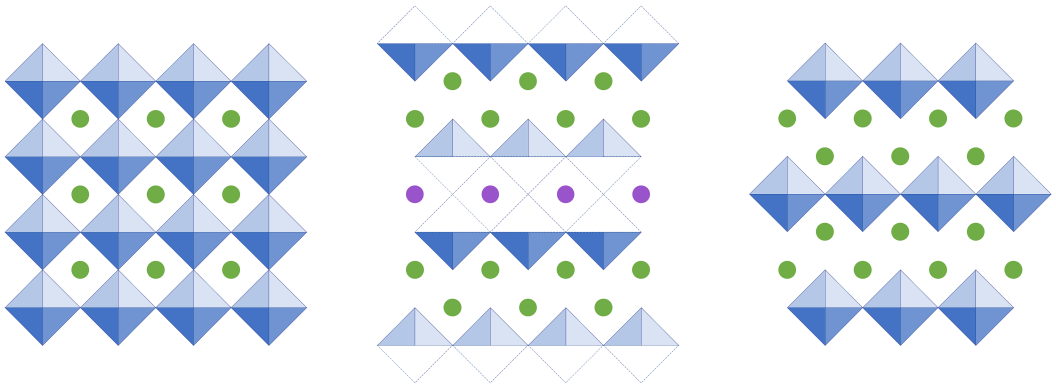

$LaCuO_3$ $La_2CaCu_2O_6$ La_2CuO_4

Figure 2.2: The examples of crystal structures of the materials from LCO structure family. CuO_6 octahedra (blue squares) are ordered in perovskite layers and intercalated with La (green circles) and Ca (purple circles).

2.2 Phases

Aside from superconductivity, cuprate materials exhibit a wide range of phases, including antiferromagnetic insulator, Fermi liquid, strange metal, charge- and spin-density wave, as well as a widely known pseudogap phase [2]. An example phase diagram is provided on Figure 2.3.

These phases are strongly dependent on electron concentration. It is usually varied by changing the composition of a material. If electron concentration needs to be decreased, it may be done by varying Oxygen stoichiometry in the compound. Being an electronegative atom, Oxygen attracts electrons from the CuO_2 plane, which is usually understood as holes introduced to the plane [14]. Alternatively, electron concentration can be increased by replacing some of the metal ions with higher-valence ions [15]. Excess electrons are donated to the CuO_2 plane, while the remaining electrons form a stable shell.

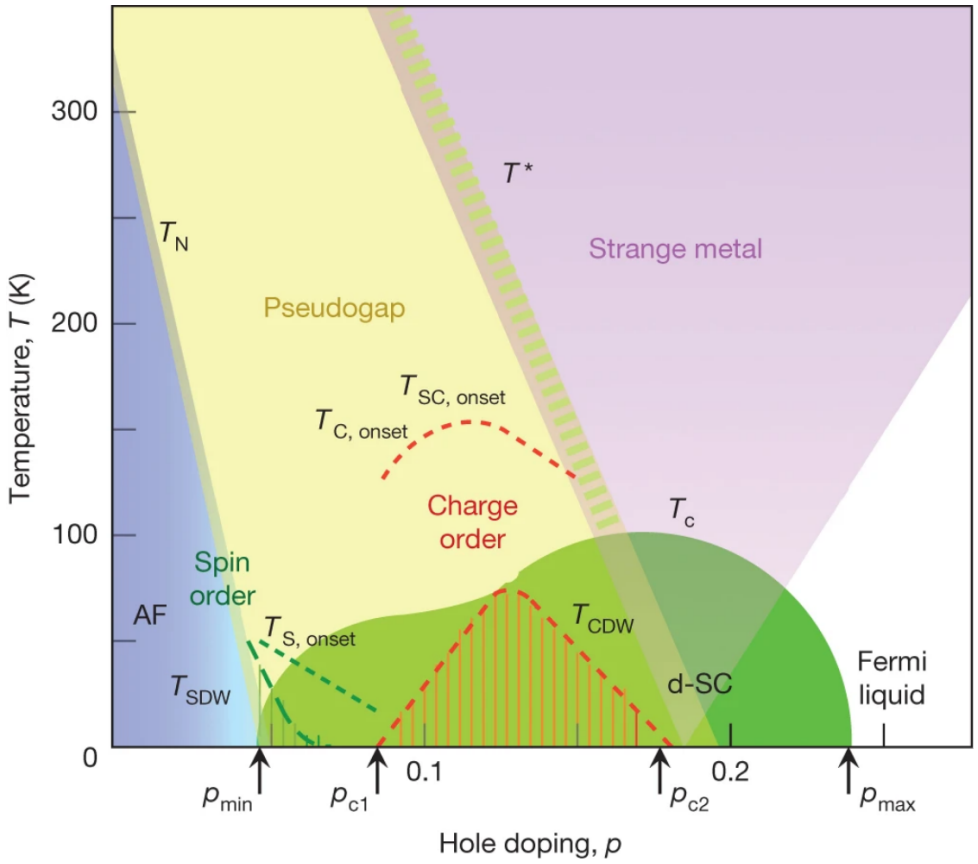

Figure 2.3: Generalized phase diagram of electronic states in hole-doped cuprate superconductors. At low hole doping, the antiferromagnetic phase (AF, blue region) is observed. When the doping is increased, multiple other phases can be observed depending on the temperature: superconducting phase (SC, green region), pseudogap phase (yellow), strange metal (purple), Fermi liquid (white), charge order (red) and spin order (dark green). Superconducting phase is limited to low temperatures and an interval of possible dopings, forming a so-called "superconducting dome" on the diagram. The onset of charge and spin order is detected around the fully ordered state, and is signified by the dashed lines. Reprinted by permission from [2].

2.3 LNSCO

Nd-doped La-Sr-Cu-O, also known as Nd-LSCO or LNSCO, belongs to the family of LCO superconductors [16]. Here, the spacer layers are composed of La ions, some of which are replaced with Sr or Nd ions via chemical doping. Each CuO square has a rare earth cation above and below its center, while each Cu ion is surrounded by six Oxygen ions, four of them in plane and two of them above and below the Copper ion. Therefore, there are two ways of looking at the structure:

- "from the point of view of Cu", as CuO_6 octahedra, assembled into planes and separated by La/Sr/Nd ions, commonly used in the relevant literature (Figure 2.4a),
- "from the point of view of La", as pyramids based on Cu_4O_4 square and additional O at the apex, with La/Sr/Nd ion in the center, used in this thesis (Figure 2.4b).

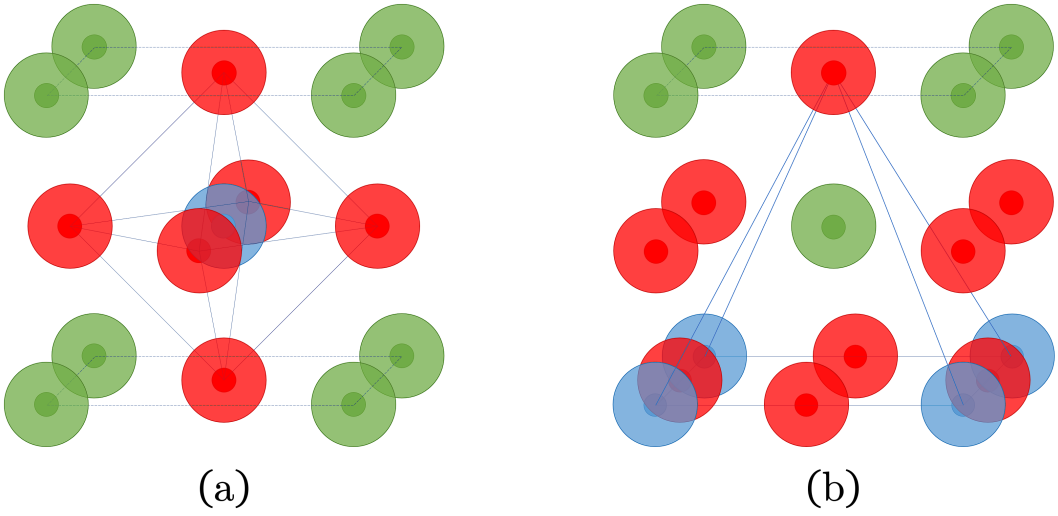

Figure 2.4: LNSCO structure from the different viewpoints: (a) from the point of view of Cu, (b) from the point of view of La. Blue circles symbolize Cu ions, red – O ions, green – rare earth ions.

The former is commonly used while describing the structural phases of the material, while the latter is suitable for perceiving the local symmetry of a rare earth ion.

2.4 Temperature dependence

When the temperature of the material changes, it transitions between three distinct structural phases: high temperature tetragonal (HTT), low temperature orthorombic (LTO), and low temperature tetragonal (LTT) (see Figure 2.5).

If speaking about electron density order phases, in addition to the antiferromagnetic insulator, pseudogap, CDW and others mentioned above, LNSCO exhibits so-called stripe ordering, as well as electron nematic order [3]. Their cause is currently unknown, and this study is one of the many studies which aim to understanding these phenomena.

It is hypothesized that the temperature dependencies are connected to the spacer layer atoms. The reasoning is based on a fact that lowest excitation energies of the CuO_2 electrons are orders of magnitude higher than k_BT, while for the spacer atoms that is not the case. Commonly, the eigenstates of free spacer atoms are highly degenerate. The multielectron ground state of Nd^{3+} is a ${}^4I_{\frac{9}{2}}$ multiplet, and the lowest excited state is ${}^4I_{\frac{11}{2}}$, 200 meV higher in energy. When an atom is embedded into a crystal, the degeneracy can be (partly) lifted, introducing low-energy excitations that can be populated by electrons via thermal distribution. These excitations can be caused by different effects, such as:

- electric field,
- magnetic field,
- exchange interaction,
- orbital hybridization.

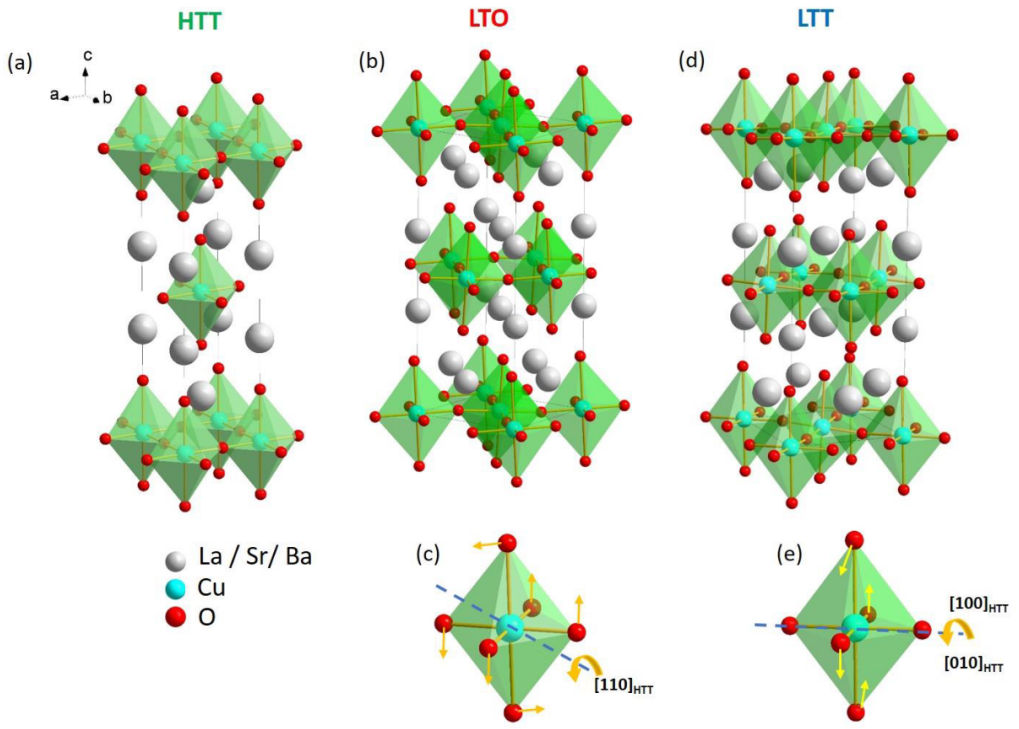

Figure 2.5: The structural phases of LNSCO: (a) HTT, (b) LTO, and (c) LTT. (a) At high temperature, L(N)SCO has a tetragonal structure. All CuO_6 octahedra are perfectly aligned. (b) When the temperature is decreased, the CuO_6 octahedra start tilting with respect to the [110] direction. The material undergoes the second-order phase transition, lowering the symmetry and increasing the size of an elementary cell. (c) Further cooling leads to another phase transition: in the LTT phase, the octahedra are tilting with respect to [100] and [010] directions. Since it is not continuously connected to LTO phase, this phase transition is of the first order [17]. In the LTT state, the tilting directions alternates between the neighbouring layers. Reprinted with permission from [16].

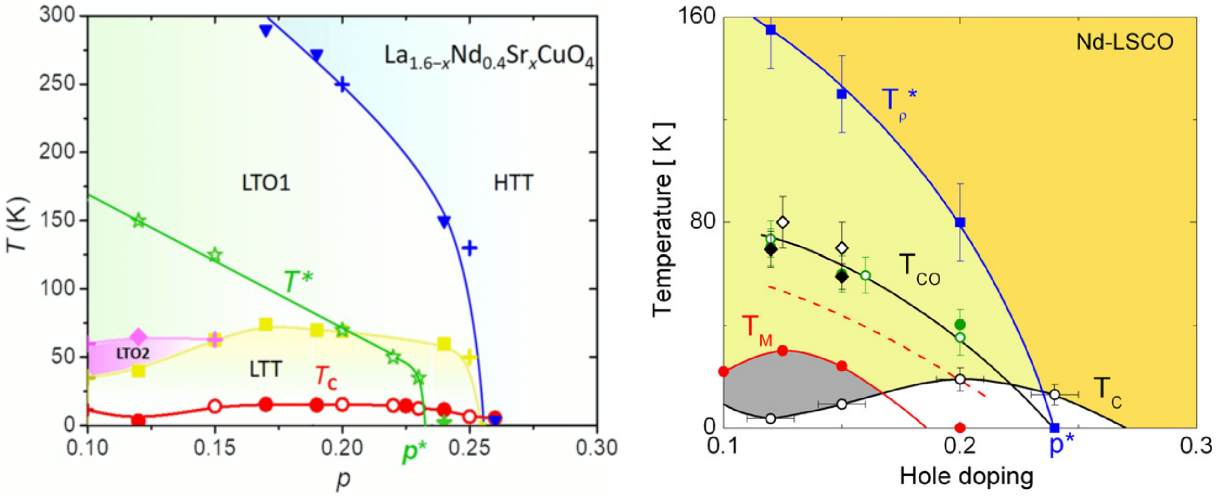

(a) Structural phase diagram

(b) Electronic phase diagram

Figure 2.6: Nd-LSCO phase diagrams. (a) Structural phase diagram. p corresponds to hole concentration, which is (ideally) given by Sr doping. T^* signifies the onset of a pseudogap phase. LTO2 is another structure phase, similar to LTO but with an additional tilt with respect to [1-10] axis. Reprinted with permission from [16]. (b) Temperature-doping phase diagram of Nd–LSCO showing the superconducting phase below T_c (open black circles) and the pseudogap region delineated by the crossover temperature T_ρ^* (blue squares). The region where static magnetism is observed is shown as a dark grey area below the T_M line (red circles), and charge order is detected below T_{CO} (black diamonds and green circles). The red dashed line shows the onset of spin modulation as detected by neutron diffraction. Reprinted with permission from [18].

Chapter 3

x-ray absorption spectroscopy

3.1 Introduction

x-ray absorption spectroscopy was developed after several ground-breaking discoveries of 1890–1910 years. The discovery of x-rays coined the research of the inner structure and properties of solids using x-ray diffraction. The discovery (and explanation) of photoelectric effect led to understanding the structure of atoms, even though only few outermost electron energy levels (orbitals with the highest energy) were accessible with it. The combination of both, called x-ray absorption spectroscopy, established a path to deeper understanding of atoms by targeting core energy levels. In 1913, just 18 years after Roentgen's discovery of x-rays and 8 years after Einstein's explanation of a photoelectric effect, the first x-ray absorption spectrum was obtained by Maurice de Broglie. Since then, both theoretical and experimental aspects have been substantially enhanced, making XAS a superior tool for the study of condensed matter systems [19].

3.2 Theoretical background

When a high-energy photon is absorbed by an atom or an ion, it can excite one of the electrons to some higher-energy state. If the photon's energy is higher than the binding

energy of an electron, the latter is completely removed from the atom. If the photon's energy is less, it is instead excited to one of the unoccupied states. Since energy levels are discrete, only those photons are absorbed whose energy is precisely equal to the energy difference between the initial and final states. Moreover, the transitions are further limited by selection rules according to a specific approximation. In the simplest case – electric dipole approximation – azimutal quantum number can only change by ± 1, and magnetic quantum number – by 0 or ± 1. By probing the atom with a radiation within some frequency range, one can produce an absorption spectrum.

Commonly, optical and ultraviolet light are enough to remove a valence electron from the outermost energy levels. This is known as photoelectric effect, which is utilized as a tool to study the valence states. If the energy of the probing photon is gradually increased, the absorption peaks are observed as electrons are excited to high energy unoccupied states Figure 3.2). A series of peaks are observed for each occupied energy level. When the photon energy reaches the binding energy of a particular energy level, a sharp absorption peak is observed. It is known as absorption edge, and labelled correspondingly to the energy level from which the electron had been excited. To excite a core electron, energies of the order of 100 to 1000 eV are required. If the occupied energy levels are known from absorption edges or some other techniques, with XAS, one can explore the unoccupied energy levels, which are considered important in some cases.

In this thesis, I examine how x-rays excite an electron from $3d$ occupied levels to $4f$ unoccupied levels. The usual excitation energy for this transition is around 1000 eV. $4f$ orbitals are considered to be localized on the atom. This way, the transition to $4f$ can be used to study the effects on a single atom, rather than in a whole crystal. It is sensitive to effects like crystal field, exchange and others.

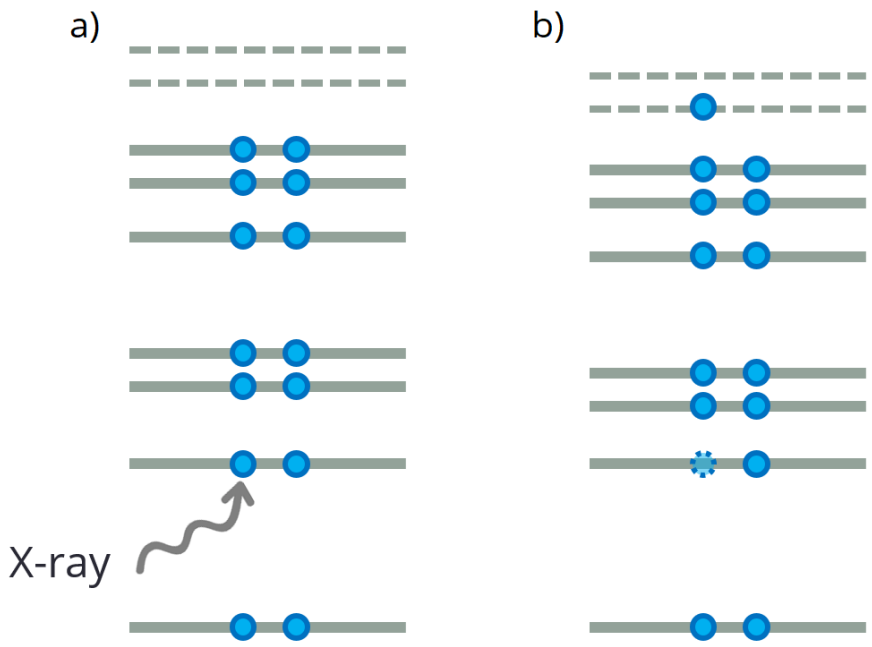

Figure 3.1: x-ray absorption model for a multi-electron atom. (a) Prior to the photon's impact, an atom is in a probabilistic mixture of states, the most probable of which is a groundstate. In a groundstate, electrons occupy the available orbitals starting from a state with the lowest energy. (b) After the impact, one of the core electrons is excited to a higher-energy state, while introducing a hole on its core level. Compared to the groundstate, energy levels are somewhat lowered because of a Coulomb attraction to the introduced hole.

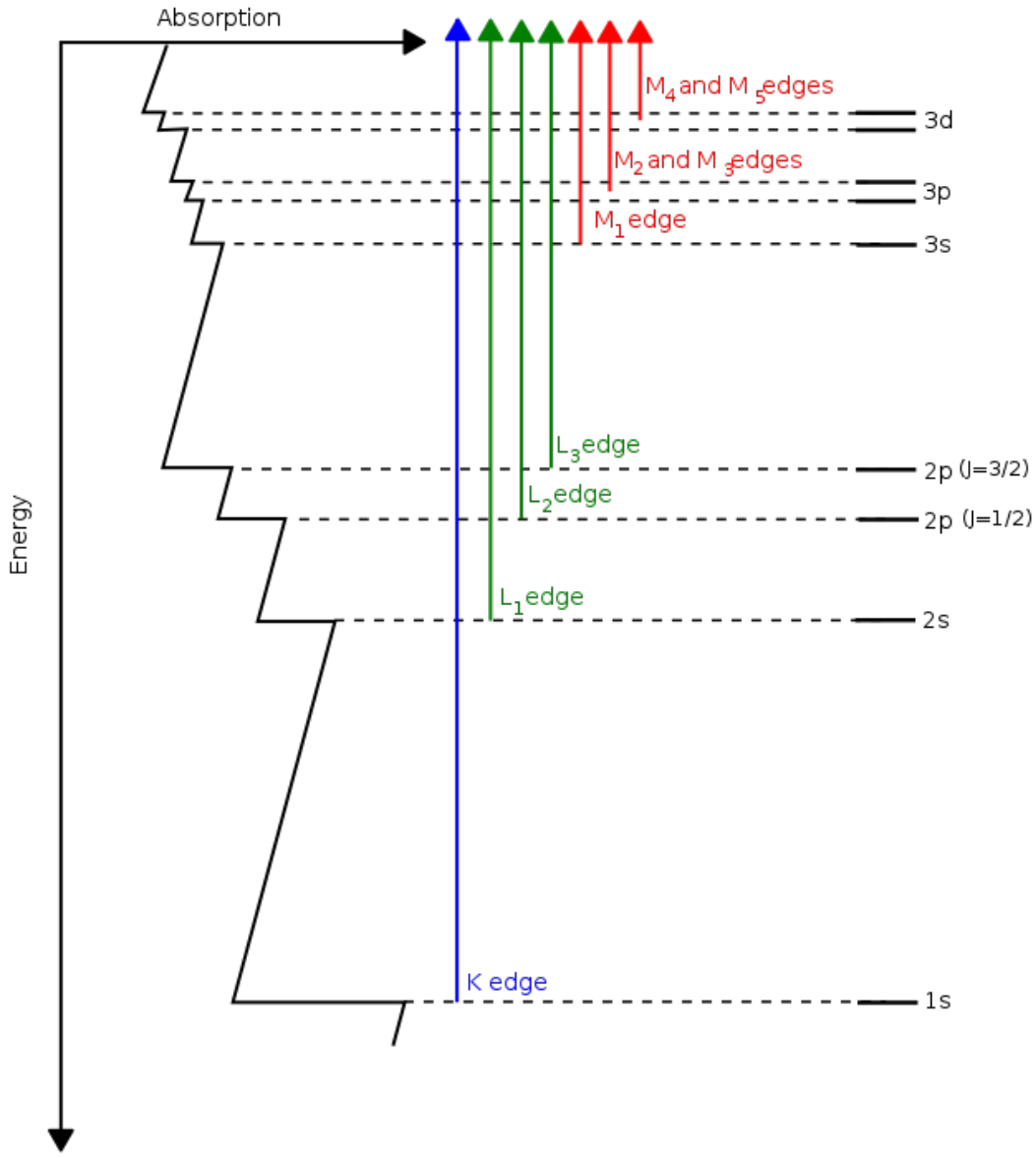

Figure 3.2: x-ray absorption edges. When the photon energy reaches the binding energy of a particular energy level, a sharp absorption peak is observed. For each initial energy level, there are multiple possible final energy levels. Thus, there are multiple peaks for the transitions *from* the given level, and they form a series corresponding to it.

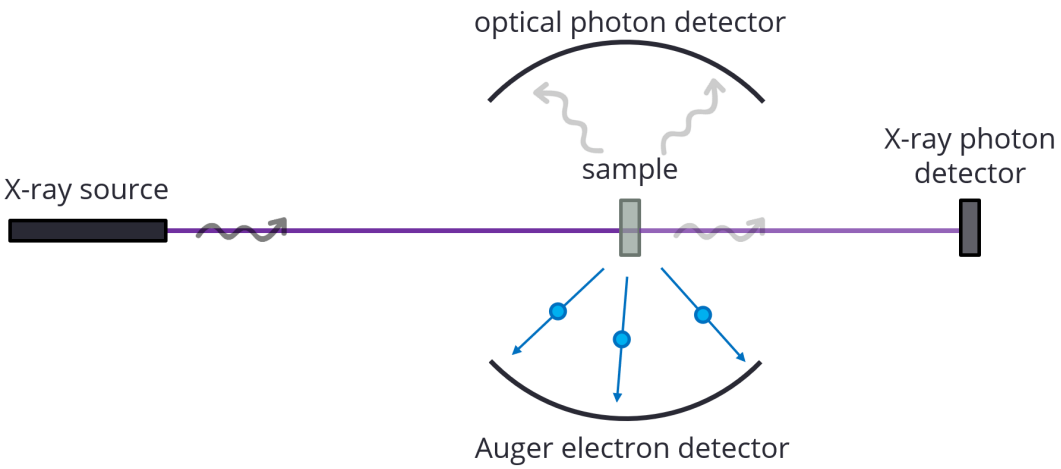

Figure 3.3: Simplistic model of an x-ray absorption measurement. When x-rays interact with a sample, some part of the radiation is absorbed, while another part is transmitted and/or reflected. Absorbed energy can be radiated via photoluminescence, giving the opportunity to detect the photoluminescence photons and thus indirectly measure the absorption. Alternatively, the energy can be released via emitting Auger electrons, which gives rise to another measurement technique. Usually, total count of emitted particles is measured, although their angular distribution contains additional information and can be measured as well.

3.3 Experimental technique

3.3.1 X-ray generation

Experimentally, XAS are measured in synchrotrons, like BESSY [20], CLS [21] etc. There, electrons are accelerated to energies on the order of GeV, typically by using a ring accelerator. There, electrons follow a closed loop path which necessary requires velocity direction change. This acceleration is applied by so-called bending magnets, which deviate the electron beam from going straight using magnetic field. Because the electrons undergo acceleration, they generate x-rays due to the bramssterhlung effect, having a continuous spectrum. To utilize it for XAS measurements, a certain frequency must be selected in a tunable manner. The devices which are able to do so are called “monochromators”.

Another technique utilizes linear periodic magnetic arrays. They are usually made from permanent magnets with the neighbouring layers rotated by 90 degrees with respect to each other. When moving through this array, electrons experience transverse periodic oscillations. These oscillations lead to strongly polarized emitted radiation. The magnetic arrays can work in two regimes:

- a strong regime, also known as "wiggler" (Figure 3.4a), which produces continuous spectrum with a fan-like intensity distribution with respect to the electron ray direction;
- a weak regime, also known as "undulator" (Figure 3.4b), which results in a coherent superposition of emitted x-rays and therefore a radiation with a line spectrum and narrow intensity distribution. Depending on regime's parameters, undulators may also produce higher harmonics.

The second regime also allows to arbitrary set a polarization of emitted x-rays by mechanically shifting the parts of the magnetic arrays longitudinally with respect to each other.

3.3.2 Absorption measurement

x-ray absorption can be measured in two ways: directly and indirectly.

Historically, the first version of XAS measuring technique was the direct measurement. For a direct measurement, the sample is placed between an x-ray source and an x-ray detector. The detector measures the intensity of the radiation transmitted through the sample, and an absorption profile is determined by dividing the attenuated spectrum by the unattenuated one. The specific attenuation is usually high, so the samples are required to be very thin, which is often impractical.

Alternatively, the XAS may be determined indirectly. The radiation absorbed by the atoms can be released with via luminescence, emitting a photon, or via Auger process, emitting an electron. The particle yield can be measured, thus making the total fluorescence yield (TFY) and total electron yield (TEY) techniques correspondingly. These

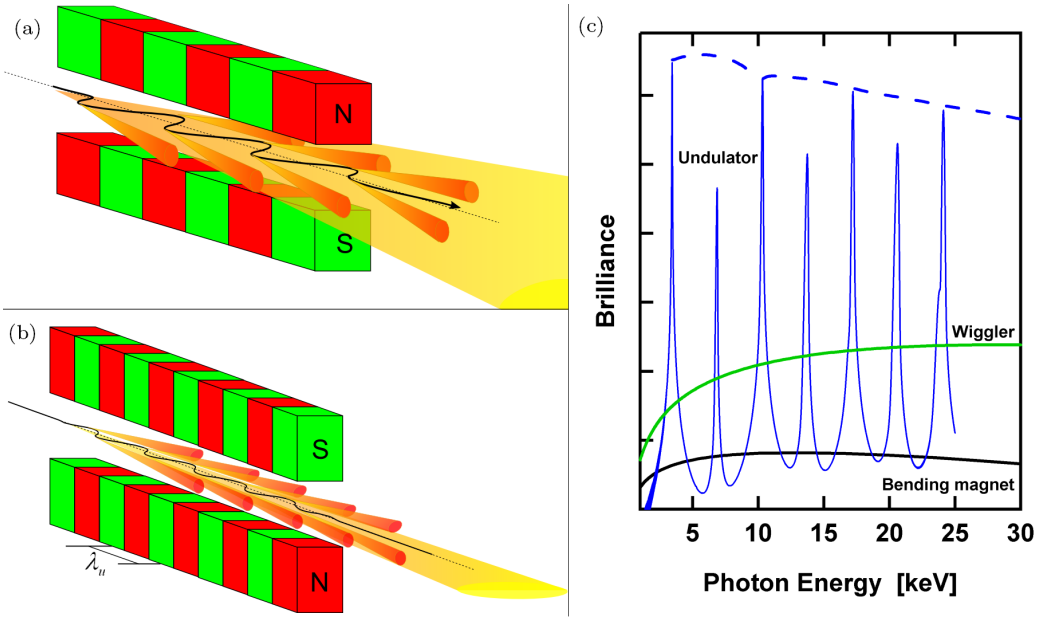

Figure 3.4: (a,b) Schematic structures of magnetic arrays used for x-ray generation: (a) wiggler, (b) undulator. Wiggler essentially behaves as a series of bending magnets, while undulator aims to create a coherent superposition. (c) spectra of x-ray generation devices. Wiggler spectrum is similar to the bending magnet spectrum, while undulator spectrum consists of narrow peaks.

techniques give more freedom in the choice of sample thickness, but require good quality of the probed surface.

3.3.3 Temperature dependency of absorption spectra

The multi-electron nature of ions gives rise to a multitude of different possible states of a single ion. These multi-electron states are characterised by their orbital momentum L, spin momentum S, total angular momentum J and total angular momentum projection M_J. For zero temperature, the electronic state of an ion can be described as a set of one-electron orbitals populated by electrons with accordance to the Hund's rules:

1. Groundstate of an ion maximizes total spin angular momentum S and the number

of unpaired electrons;

2. For a given S, groundstate maximizes orbital angular momentum L;

3. For a given combination of L and S, groundstate minimizes total angular momentum J for an ion with less-than-half-filled outermost subshell (and maximizes J for an ion with more-than-half-filled outermost shell).

For non-zero temperatures, states with multiple different electron distributions are possible.

Each of those multi-electron states may have a distinct energy. From each particular state, there are plenty of other states with higher energy, and thus plenty of possible transitions to those states. Some of the transitions are forbidden within dipole approximation, leaving the distinct spectrum of possible transitions for each distinct state.

An ensemble of ions with non-zero temperature can be represented as a statistical mixture of ions in different states. Statistical weight of a particular state within the ensemble can be determined by Boltzmann distribution (also known as Gibbs distribution). If a transition spectrum is now measured, it is presented as a weighted average of spectra of different possible states, with the statistical weight equal to a Boltzmann coefficient of a corresponding state. Change of the temperature leads to rebalancing of statistical weights of possible states, thus changing the resulting spectrum (Figure 3.5).

3.3.4 Characteristic tensors

If the incoming electromagnetic radiation is polarized, the intensity of absorption may depend on the direction of polarization. Photon absorption corresponds to the transition of an electron from $3d$ to $4f$ quantum state. The intensity of absorption is captured by a conductivity tensor $\sigma(\omega)$:

$$I_{\text{abs}}(\omega) = -\text{Im}\left[\sum_i \epsilon^* \sigma_i(\omega)\epsilon\right], \tag{3.1}$$

where ϵ denotes the polarization vector, and i runs over all atoms in the sample. At the same time, the atomic scattering factor is defined as:

$$f = \epsilon^*_{out} F_n(\omega) \epsilon_{in}, \tag{3.2}$$

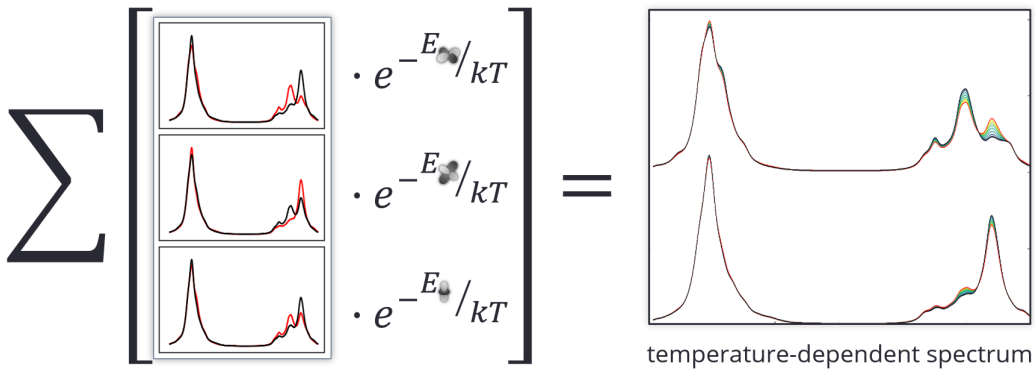

Figure 3.5: In an ensemble of identical ions, the ions can be in different possible states. Those states can have different spectra, and thus the spectrum of a whole ensemble is a weighted average of individual spectra, which changes with temperature.

where ϵ_{in} and ϵ_{out} are the incoming and outcoming polarization directions, and $F_i(\omega)$ is a scattering tensor, proportional to the conductivity tensor:

$$F_i(\omega) \propto \omega \cdot \sigma_i(\omega) \tag{3.3}$$

Scattering intensity depends on atomic scattering factor:

$$I_{\text{scatt}}(\omega) = \left| \sum_i e^{i\,\Delta \boldsymbol{k} \cdot \boldsymbol{r}_i} f_i \right|^2, \tag{3.4}$$

where $\boldsymbol{r}_i$ indicates the position of the i-th atom.

This draws a link between x-ray absorption and x-ray scattering [22]. By studying the x-ray absorption spectrum, we would be able to recover the tensor and thus study the behaviour of the atomic scattering factor.

In case of Nd-LSCO, the Nd^{3+} ions are layered in planes, parallel to a and b crystallographic directions. In the LTT phase, the tilting direction of the CuO_6 octahedra alternates in the neighbouring layers, it can be expected that the horizontal axes of symmetry for the Nd^{3+} ions would alternate between layers as well. Thus, when the absorption is measured with polarization parallel to a axis, half of the ions would be contribute according to σ_{xx}

component, and another half – to σ_{yy} component:

$$I_{\text{abs}}(\omega) \propto -\text{Im}\Big[\sigma_{xx}(\omega) + \sigma_{yy}(\omega)\Big], \tag{3.5}$$

When the scattering is measured in (001) direction, the contributions of the neighbouring layers have phases which differ by $\Delta\boldsymbol{k} \cdot \boldsymbol{r} = \pi$. Thus, the scattering intensity would be proportional to the difference between horizontal components of the single-ion scattering tensor [3]:

$$I_{\text{scatt}}(\omega) \propto \Big|f_{xx}(\omega) - f_{yy}(\omega)\Big|^2, \tag{3.6}$$

3.3.5 Linear dichroism

The wavefunctions of a free ion are spherically symmetrical, and the absorption appears uniform. If, however, the ion is not free, that is, affected by some external field or interaction, the symmetry of both the initial and the final state is imposed by this field. Thus, for the incoming radiation with different polarization, the absorption spectrum may differ. This effect is known as dichroism, which is called correspondingly to the polarization type (linear or circular).

Historically, dichroism has been firstly observed in natural gemstones such as tourmaline for visible light (e.g. Figure 3.6). Later, it has also been discovered for x-ray range, as well as for other parts of electromagnetic radiation and for many other wave processes (e.g. spin-wave directional dichroism [23] or acoustic helical dichroism [24]). There are two techniques which use linear dichroism of x-rays:

- x-ray magnetic linear dichroism (XMLD), where the measured dichroism is induced by an external magnetic field, and
- x-ray natural linear dichroism (XNLD), where the measured dichroism is caused by the intrinsic properties of a material.

XMLD has been used to study phenomena such as exchange biasing and magnetic anisotropy. XNLD, on the other hand, provides information on the structure of a material:

if an ion has highly anisotropic wavefunctions, it exhibits pronounced dichroism. Thus, local anisotropy can be studied with this technique.

Figure 3.6: An example of optical dichroism in tourmaline. Photos are taken from the same spot and angle with the same illumination, but with the different orientation of the camera's polarizing filter. For one polarization, light absorption by the tourmaline crystal is stronger than for a perpendicular polarization, and the crystal appears darker. Reprinted from Wikimedia.

Chapter 4

Crystal field theory

4.1 Introduction

Crystal field theory describes ions within a crystal. If the electrons of an ion are localized on it, crystal field theory suggests that an ion within a crystal can be modeled as a free ion perturbed by an effective external electric field, *acting in the form of a one-electron potential* [6, 7]. This concept has been fairly successful in simulating the energy level spectrum, as well as expectation values.

Even though the crystalline electric field (CEF) is an *effective* field, it can be conceptualized as an electric field originating from the neighbouring ions. Usually, the closest atoms are taken into account as electron clouds, while further atoms are approximated by point charges. This picture allows one to numerically calculate the CEF configuration on an ion site "from first principles". Alternatively, the configuration can be determined phenomenologically, i.e. by fitting the parameters so that the calculated properties of the system correspond to the experimentally measured properties. If the parameters derived from the theory are compared to the parameters fitted to the experiment, the former appear to be overestimated, sometimes by several times in magnitude; however, the general picture still holds close to the experimentally observed.

4.2 Crystal field theory Hamiltonian

Let us recall the fundamental assumption of crystal field theory: the bound ion can be described as a free ion within an external field, acting on the electrons in the form of a one-electron potential. In addition, due to the screening effect, shell electrons define most of the properties, and a full set of electrons can be replaced by just the outer shell, or by the outer shell and a core level that takes part in the studied phenomenon. Therefore, the crystal field Hamiltonian can be written as[1]:

$$H_p + H_k + H_{CR} + H_{So} + H_{CF}, \tag{4.1}$$

where each of the terms is written as a sum of one-electron operators, corresponding to the i-th electron, over the considered shells filled in total with N electrons. These terms correspond to:

- spherically symmetric potential energy in a screened nuclear potential:

$$H_p = -\sum_i^N V(r_i), \tag{4.2}$$

  where $V(r_i)$ denotes the potential for the i-th electron located at r_i from the nucleus;

- kinetic energy:

$$H_k = -\sum_i^N \frac{\nabla_i^2}{2} \tag{4.3}$$

- Coulomb repulsion between different electrons:

$$H_{CR} = \sum_{i>j}^N \frac{1}{r_{ij}} \tag{4.4}$$

- spin-orbit coupling:

$$H_{So} = \sum_i^N \zeta_{na} \mathbf{l}_i \cdot \mathbf{s}_i \tag{4.5}$$

[1]Here and below, Hamiltonian terms are given in atomic units.

- effective crystal electric field:

$$H_{CF} = W_{CF} = -\sum_{i}^{N} V_{CF}(\mathbf{r}_i), \tag{4.6}$$

where $V_{CF}(\mathbf{r}_i)$ denotes the effective one-electron potential for the i-th electron.

If the external magnetic field $\boldsymbol{B}$ is applied, a Zeeman term is added to the Hamiltonian:

$$H_{Ze} = \mu_{\mathrm{B}} \boldsymbol{B} \cdot (2\boldsymbol{S} + \boldsymbol{L}) \tag{4.7}$$

If an ion is magnetic, the exchange interaction is added as an effective magnetic field $\boldsymbol{B}_{\mathrm{eff}}$, acting on the spin only:

$$H_{ex} = \mu_{\mathrm{B}} \boldsymbol{B}_{\mathrm{eff}} \cdot \boldsymbol{S} \tag{4.8}$$

4.3 Crystal electric field potential

As mentioned above, the effective CEF potential is assumed to originate from the neighbouring ions. If we also assume that the ion's electrons do not change the external charge density $\rho(\mathbf{R})$, the one-electron potential V_{CF} for an electron located at $\mathbf{r}$ can be written as:

$$V_{CF}(\mathbf{r}_i) = \int \frac{\rho(\mathbf{R})}{|\mathbf{r}_i - \mathbf{R}|} d\mathbf{R} \tag{4.9}$$

Here, $\mathbf{R}$ runs over the space around an ion ($|\mathbf{R}| > |\mathbf{r}|$).

This potential can be expanded as a series on spherical harmonics:

$$\frac{1}{|\mathbf{r} - \mathbf{R}|} = \frac{1}{R} \sum_{l} \left(\frac{r}{R}\right)^{l} P_l(\cos\theta) \tag{4.10}$$

where $P_l(\cos\theta)$ denotes Legendre polynomial:

$$P_l(\cos\theta) = \frac{4\pi}{2k+1} \sum_{m=-l}^{l} (-1)^m Y_l^m(\theta_r, \phi_r) Y_l^{-m}(\theta_R, \phi_R) \tag{4.11}$$

This expansion leads to the famous Wybourne notation:

$$V_{CF}(\mathbf{r}_i) = \sum_{k,q \leq k} B_{k,q} C_q^k(\theta_i, \phi_i) \tag{4.12}$$

where C_k^q denotes the so-called "semi-normalized spherical harmonics" defined as:

$$C_k^q(\theta, \phi) = \sqrt{\frac{4\pi}{2k+1}} Y_k^q(\theta, \phi) \tag{4.13}$$

However, alternative parameterizations also exist. The so-called BST (Buckmaster-Smith-Thornley) parameterization makes use of Stevens operator equivalents. If the study is limited only to the lowest multiplet with common J, the CEF potential can be drastically simplified. According to Wigner-Eckart theorem, the operators depending on Cartesian coordinates x, y, z can be replaced by equivalent operators expressed in terms of polynomials in $J_{x,y,z}$ operators:

$$\hat{O}(x, y, z) = \theta_l \hat{O}(J_x, J_y, J_z) \tag{4.14}$$

Here, the equivalent operator $\hat{O}(J_x, J_y, J_z)$ can be constructed by directly replacing free x, y, z with $J_{x,y,z}$ respectively, and the products of x, y, z with symmetrized products[2] of $J_{x,y,z}$. θ_l is a proportionality factor which depends on the orbital quantum number of the unfilled shell, the number of the electrons in this shell, and the total angular momentum. It is usually denoted α_J for $l = 2$, β_J for $l = 4$ and γ_J for $l = 6$. These parameters are calculated for common rare earth ions, and can be found in many classic works, for example, in Refs. [7, 6, 25, 26].

In contrast to the Wybourne parameterization, where the potential is expressed for each individual electron using their coordinates, Stevens operators $\hat{O}_q^k$ are expressed in terms of $\hat{J}_{x,y,z}$ which act on the $4f$ shell as a whole, eliminating the need for taking a sum over all electrons. The complete list of Stevens operators can be found in [25]. The crystal field term in the Hamiltonian is then written as:

[2]Symmetrized product is a sum of all the possible combinations of $J_{x,y,z}$ with the same power, divided by the number of these combinations. For example, a symmetrized product of J_x and J_y is constructed like $(J_x J_y + J_y J_x)/2$.

$$H_{CF} = \sum_{k,q} A_q^k \langle r^q \rangle \theta_q \hat{O}_q^k(\hat{J}_z, \hat{J}_\pm), \tag{4.15}$$

or simply

$$H_{CF} = \sum_{k,q} B_q^k \hat{O}_q^k(\hat{J}_z, \hat{J}_\pm), \tag{4.16}$$

where

$$B_q^k = A_q^k \langle r^k \rangle \theta_k \tag{4.17}$$

The values of $\langle r^k \rangle$ are calculated for common rare earth ions and are often provided with θ_l, as they are, for example, in Ref. [26], page 594. However, they are usually not used independently from A_q^k: Stevens crystal field parameters are almost always given as either $A_q^k \langle r^k \rangle$ or B_q^k.

The conversion between the Stevens and Wybourne parameters can be done using the parameter $\lambda_{k,q}$:

$$\lambda_{k,q} = \frac{\text{Stevens } A_q^k \langle r^k \rangle}{\text{Wybourne } B_{k,q}} \tag{4.18}$$

This parameter is given, for example, in Ref. [6], page 32. As an alternative, $1/\lambda_{k,q}$ parameters are given in Ref. [7].

For numerical computation, it is useful to convert this expression using second quantization. Then, the crystal field term can be written as

$$H_{CF} = \sum_{\tau_1, \tau_2} \langle \phi_{\tau_1}(\mathbf{r}) | V(\mathbf{r}) | \phi_{\tau_2}(\mathbf{r}) \rangle \, a_{\tau_1}^\dagger a_{\tau_2} \tag{4.19}$$

where τ denotes the combination of quantum numbers (n, l, m_l), ϕ_τ denotes the corresponding spherical harmonic, and a_τ and $a_\tau^\dagger$ denote the ladder operators for an electron

in a corresponding state [26]. By separating the spherical harmonics into radial and angular parts and using the expansion 4.12, the crystal field term can be converted to next expression:

$$H_{CF} = \sum_{\tau_1,\tau_2} \sum_{k,m} A_{k,m} \langle Y_{l_1,m_1} | C_{k,m} | Y_{l_2,m_2} \rangle \, a^{\dagger}_{\tau_1} a_{\tau_2} \tag{4.20}$$

Here, all the radial-dependent part is absorbed into a parameter set $A_{k,m}$, which is commonly acting as a set of fitting parameters.

In the case of Neodymium, the outer shell is composed of $4f$ electrons. Due to the symmetry of the wavefunction, the number of non-zero crystal field parameters is limited by the terms with $k < 2l$ and $q <= k$. Moreover, local symmetry of an ion can further eliminate the parameters with mismatching symmetry [25]:

- if there is a center of inversion on ion site, the parameters with odd k vanish (corresponding spherical harmonics do not have inversion symmetry);
- if the z-axis is not an m-fold rotation axis, the parameters with $q = m$ vanish.

In the idealized case of LNSCO, the local symmetry of Nd^{3+} ion is C_{4v}, or square pyramid symmetry. This group has four-fold rotational symmetry with respect to the vertical axis. It means that:

- due to the symmetry of the $4f$ wavefunction, $k < 6$ and can only be even:

$$k = 2, 4, 6 \tag{4.21}$$

- due to the local symmetry of an ion, q is limited by the four-fold symmetry:

$$q = 0, 4 \tag{4.22}$$

Therefore, only five CEF parameters which satisfy these constraints occur in the Hamiltonian:

$$B^0_2, B^0_4, B^4_4, B^0_6, B^4_6 \tag{4.23}$$

For other symmetries, the list of allowed terms is also known. The compiled table can be found, for example, in Ref. [27], page 195.

4.4 Crystal field splitting

So far only the theoretical background of crystal field was presented, but not the impact on atomic spectrum. Since the valence shell of the atom in study is a $4f$ shell, the further part will be dedicated specifically to $4f$. It is worth mentioning, though, that the influence of crystal field varies with open-shell of an atom roughly in this order: $5d > 4d > 3d > 5f > 4f$, where in each next shell the crystal field effect is approximately 10 times less pronounced due to the difference in spatial distribution of electron density of the corresponding orbitals.

The $4f$ orbital is mostly shielded from the environment by the closed shells $5s^2 5p^6$. Thus, compared to other orbitals, is exhibits a rather small overlap with neighbouring electron density. It means that the energy level structure is mostly defined by intra-atomic interactions, and the impact of the neighbouring environment can be considered as a perturbation of it.

In $4f$ systems this role is played by a spin-orbit coupling. It leads to the fine structure splitting of energy levels by quantum number J, that is, a total angular momentum. The groundstate of a spin-orbit coupled system is a multiplet with total momentum J. This state is degenerate by a number of values of total angular momentum projection J_z – a $(2J + 1)$-fold degenerate state. As an example, the ground state of Nd^{3+} is a multiplet with $J = 9/2$, which is a 10-fold degenerate state.

The crystal field effect then acts as a perturbation of this system and leads to lifting this degeneracy. The cause for the degeneracy lifting is a particular point group symmetry in which the ion is embedded, resulting in spinorbitals with different symmetries having a different energy. Depending on the point group symmetry, one multiplet with half-odd J can be divided in up to $(2J + 1)/2$ doublets, and with half-even J – into a singlet and J doublets [28]. The doublets can be further separated, for example, with Zeeman effect, by applying magnetic field to the ion.

4.5 One-electron energies

In addition to Wybourne parameters, the CEF potential can also be parameterized by energies of the one-electron eigenstates. These eigenstates can be presented as linear combinations of single-electron Hydrogen-like orbitals. Thus, these energies can be presented as linear combinations of the energies on an electron on these orbitals, which are proportional to the amplitudes of the field expanded on spherical harmonics.

Single-electron energies are usually labeled accordingly to the symmetry and the degeneracy of the corresponding eigenstates. A classic example of that is the splitting of the one-electron energies of $3d$ orbitals in a crystal field of O_h symmetry (Figure 4.1).

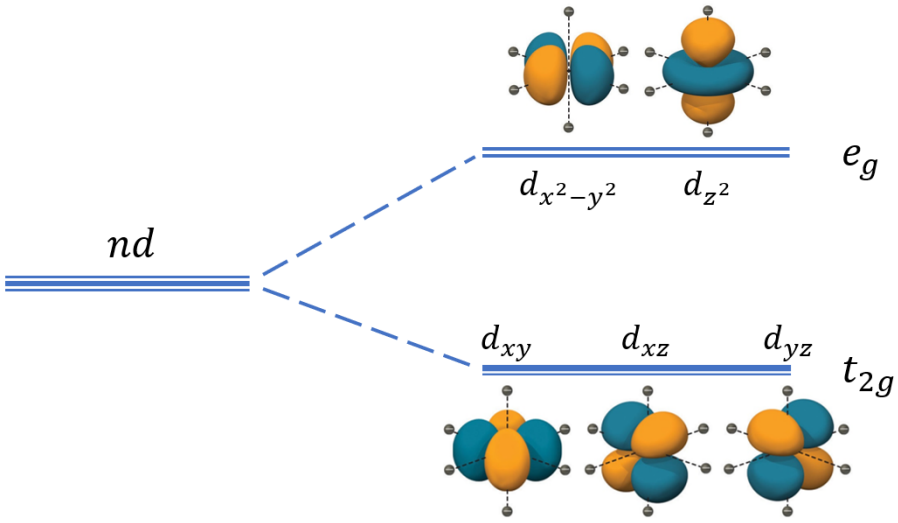

Figure 4.1: Example of crystal field splitting of $3d$ orbitals in an octahedral field. Here, the five-fold degeneracy is partly lifted, and the groundstate splits into a two-fold and a three-fold degenerate levels. Wavefunctions with lobes pointing at the neighbouring charges have their energy increased by $6D_q$, while ones with lobes pointing in between the neighbouring charges have their energy decreased by $4D_q$. In this case, the splitting energy is usually denoted as $10D_q$.

4.6 Point charge approximation

The simplest model to represent electric field in a crystal structure is the point charge approximation. In this model, ions are represented as effective point charges. Their charge and position may differ from the ones attributed to ions. If the whole lattice is taken into account, the calculated potential is then called a "Madelung constant".

This approximation works well in case of low orbital hybridization. However, this is not the case for LNSCO: due to the proximity of Copper and Oxygen energy levels, their electron states are strongly hybridized. Nevertheless, point charge model presents a valuable foundation for understanding a general picture.

One of the common techniques for calculations of point charge models is the "expanding cube" technique [29]. In this technique, the number of ions taken into account is increasing iteratively, until the values of crystal field parameters are converged. For the first iteration, only one crystal cell is taken into account. For the next iteration, nearest neighbouring cells are added into the calculation. Iterations repeat until the change in calculated values is less than a preliminarly established threshold.

Chapter 5

Quanty

The modeling is conducted using Quanty, a Lua-based quantum many body script language [8]. It provides a user with a set of tools to create and analyze wavefunctions, operators and Hamiltonians.

5.1 Basis

As basis states, Quanty utilizes one-particle modes. A single mode acts like a box in which a particle can be placed. To define a basis, the user only needs to list the indices of basis states, or even just a number of possible states.

The modes have two types: Fermionic and Bosonic.

- A Fermionic mode can correspond to a Hydrogen-like spin-orbital within a multielectron atom, or to a Wannier orbital in a solid or a molecule. Usually, Fermionic basis states are grouped into shells, similar to electron shells within a Hydroden atom, separate for spin-up and spin-down states. They are indexed by a single index τ, which corresponds to a set of four quantum numbers n, l, m and σ, where each next quantum number changes faster than the previous one.

  A Fermionic mode can either be unoccupied or occupied by a single particle.

- A Bosonic mode can correspond to a phonon mode within a solid or a molecule. Contrary to the Fermionic mode, a Bosonic mode can be occupied by 0 to 255 particles.

Of course, one-particle states are rarely used by themselves. In a multi-electron system, multi-electron basis states can be approximated by a properly chosen product of a single-electon states known as Slater determinant. For a set of n Fermionic modes $\phi_\tau(\mathbf{r})$, a Slater determinant is a basis state defined as:

$$\Phi(\mathbf{r}_0, \mathbf{r}_1, \ldots, \mathbf{r}_{n-1}) = \frac{1}{\sqrt{n!}} \begin{vmatrix} \phi_0(\mathbf{r}_0) & \phi_1(\mathbf{r}_0) & \cdots & \phi_{n-1}(\mathbf{r}_0) \\ \phi_0(\mathbf{r}_1) & \phi_1(\mathbf{r}_1) & \cdots & \phi_{n-1}(\mathbf{r}_1) \\ \vdots & \vdots & \ddots & \vdots \\ \phi_0(\mathbf{r}_{n-1}) & \phi_1(\mathbf{r}_{n-1}) & \cdots & \phi_{n-1}(\mathbf{r}_{n-1}) \end{vmatrix} \tag{5.1}$$

To speed up the computations, these determinants are never explicitly written, and are calculated only if necessary. Instead, a multi-electron basis state where electrons have indices τ_i is represented by a set of corresponding creation operators $a^\dagger_{\tau_i}$, acting on a void state:

$$\Phi(\{\tau_i\}) = \prod_i a^\dagger_{\tau_i} |0\rangle \tag{5.2}$$

By using extensive optimizations, Quanty can deal with extremely high number of states (up to 10^{100}). To implement these optimizations, all the calculations are avoiding operating with wavefunctions and Slater determinants themselves. For example, a basis state for an electron with spin-down on a p-orbital with $m_l = -1$ can be represented as a `"000010"` string.

5.2 Wavefunctions

In Quanty, multi-electron wavefunctions can be represented as a set of basis states $|\phi_i\rangle$ and corresponding pre-factors α_i:

$$|\psi\rangle = \sum_i \alpha_i |\phi_i\rangle \tag{5.3}$$

For example, a representation of a two-electron wavefunction for two electrons on a p-orbital may look like the following:

```
{ {"100001", sqrt(1/2)}, {"010010", sqrt(1/2)} }
```
(5.4)

5.3 Operators

Operators are defined using a second quantization expansion:

$$\begin{aligned} O = &\alpha^{(0,0)} 1 \\ &+ \sum_i \alpha_i^{(1,0)} a_i^\dagger + \alpha_i^{(0,1)} a_i \\ &+ \sum_{i,j} \alpha_{i,j}^{(2,0)} a_i^\dagger a_j^\dagger + \alpha_{i,j}^{(1,1)} a_i^\dagger a_j + \alpha_{i,j}^{(0,2)} a_i a_j \\ &+ \sum_{i,j,k} \cdots \end{aligned} \tag{5.5}$$

There are many built-in functions for generating standard operators, such as momentum operators (S, L, J), their projections (x, y, z), + and − versions, spin orbit coupling ($l.s$), Coulomb repulsion (U), crystal field and ligand field operators etc. Complex operators, such as spin-orbit coupling operator, can be created as combinations of simpler operators.

5.4 Crystal field operator

As mentioned in the previous chapter, crystal field can be represented as an expansion on spherical harmonics. Quanty provides a way to create a corresponding operator using a list of harmonic amplitudes accompanied by corresponding indices:

```
Hcf = NewOperator("CF", NF, IndexUp, IndexDn, Akm)
```
(5.6)

where `NF` denotes the number of fermions, `IndexUp` and `IndexDn` denote the set of indices of spin-up and spin-down states correspondingly, and `Akm` denotes a set of Wybourne $B_{k,q}$ crystal field parameters given in electronvolts (eV).

The `Akm` set can be set up manually as a list of triplets {`k, m, Akm`}. Alternatively, for some of the symmetries, the coefficients can be computed given the symmetry and splitting energies:

```
Akm = PotentialExpandedOnClm("C4v", 3, Ea2,Eb1,Eb2,Eeu1,Eeu2)        (5.7)
```

Usually, the `Akm` are taken as fitting parameters.

5.5 Spectra

Various spectra can be created by calculating the Green function for a corresponding operator. For a non-resonant simple transition operator, it can be done using `CreateSpectra()` function, which corresponds to the following quantum-mechanical expression:

$$\texttt{CreateSpectra(H, TrO, psi)} = \left\langle \psi \middle| TrO^{\dagger} \frac{1}{(\omega + i\Gamma/2 + E_0 - H)} TrO \middle| \psi \right\rangle \qquad (5.8)$$

Here, `H` denotes the Hamiltonian after the excitation, `TrO` is the dipole transition operator, and `psi` is a list of wavefunctions, corresponding to the eigenstates of the initial Hamiltonian before the transition. The transition operator sets the direction and polarization of the incoming light. The Green function is thus calculated for each wavefunction from the set, so the result is a set of corresponding Green functions. To create a final spectrum, these functions are scaled correspondingly to each wavefunction's occupation which are calculated from their corresponding energies and the temperature. The imaginary part of this weighted sum would correspond to a spectrum, calculated for particular temperature.

5.6 Demonstration

The example below illustrates how Quanty can simulate XAS of different atoms.

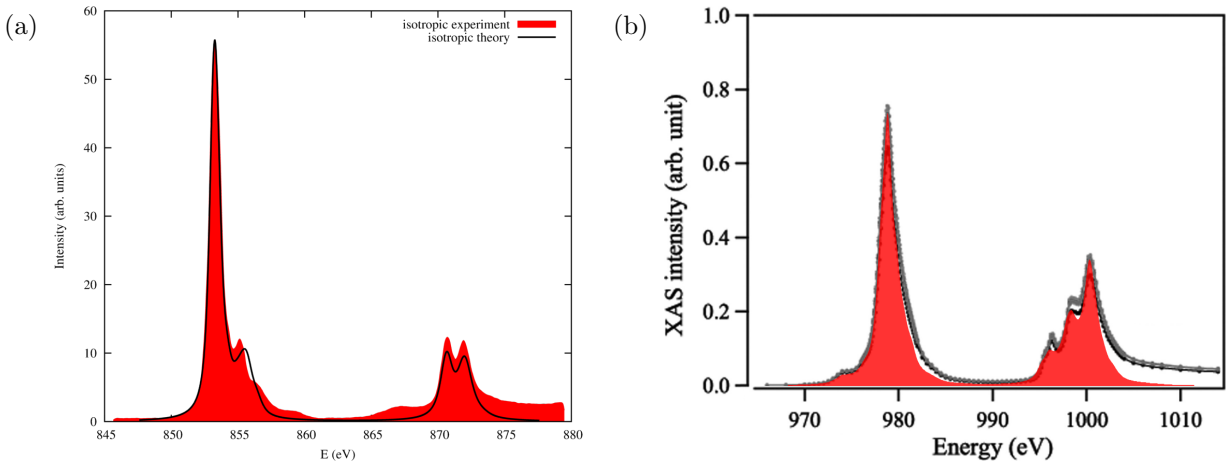

Figure 5.1: The results of modeling in Quanty show general agreement in the positions and magnitudes of the main absorption peaks when compared to experimental data. These models do not take into account the specifics of the experimental setup, crystallographic diffraction, other electrons and the interaction of the ion with the surrounding charge density, hence the differences. (a) Spectrum of Ni^{2+} in NiO, corresponding to the excitation of a $2p$ electron into a $3d$ unoccupied orbital. Black line – modeling, red area – experiment [30]. (b) Spectrum of a free Nd^{3+} ion, corresponding to the excitation of a $3d$ electron into a $4f$ unoccupied orbital. Black and gray lines – experiment, red area – modeling.

Chapter 6

Results

6.1 Experimental prerequisites

The experimental data on which this study is based consists of two data sets. Both of them studied the samples of $La_{1.6-x}Nd_{0.4}Sr_xCuO_2$ with $x = 0.125$.

The first dataset is a set of x-ray absorption spectra on $M_{4,5}$ absorption peaks (energy range 970 to 1000 eV), collected on BESSY beamline by Naman Kumar Gupta [5]. The graph is presented on a Figure 6.1.

The spectrum exhibits noticeable natural linear dichroism, which is unchanged in case if the outer magnetic field is applied (up to 6 T). It is, however, changed with temperature: with temperature increasing from 20 to 100 K, the second peak of M_4 edge is decreased, while the third one is increased.

The second dataset is the Inelastic Neutron Scattering data from Ref. [31]. There, crystal field excitations were identified with the energies of 11, 25 and 45 meV with respect to the ground state. The spectrum is pictured on Figure 6.2.

Using the scripts outlined in Appendix A, the following results were produced.

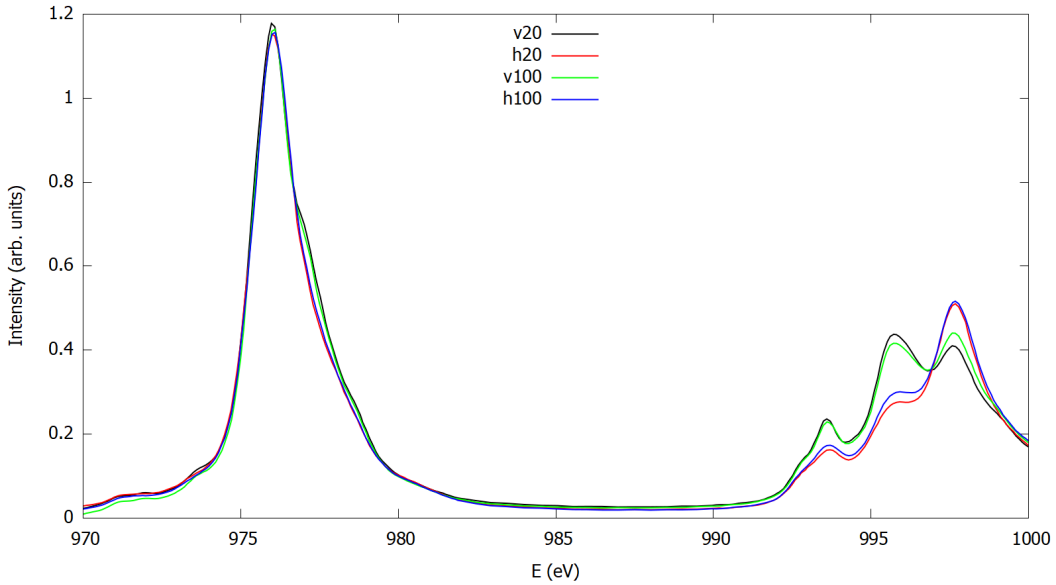

Figure 6.1: Experimental x-ray absorption spectrum of Nd^{3+} at $M_{4,5}$ edge in a $La_{1.6-x}Nd_{0.4}Sr_xCuO_4$ sample with $x = 0.12$, for two polarization directions: vertical (i.e. parallel to the c axis of a crystal, black and green lines) and horizontal (parallel to the a or b axis, red and blue lines). The difference in absorption for the two polarizations is especially noticeable for the M_4 peaks (994, 996 and 998 eV). When the temperature changes from 20 K (black and red lines) to 100 K (green and blue lines), the absorption profile changes for both polarizations. Adapted from Ref. [5].)

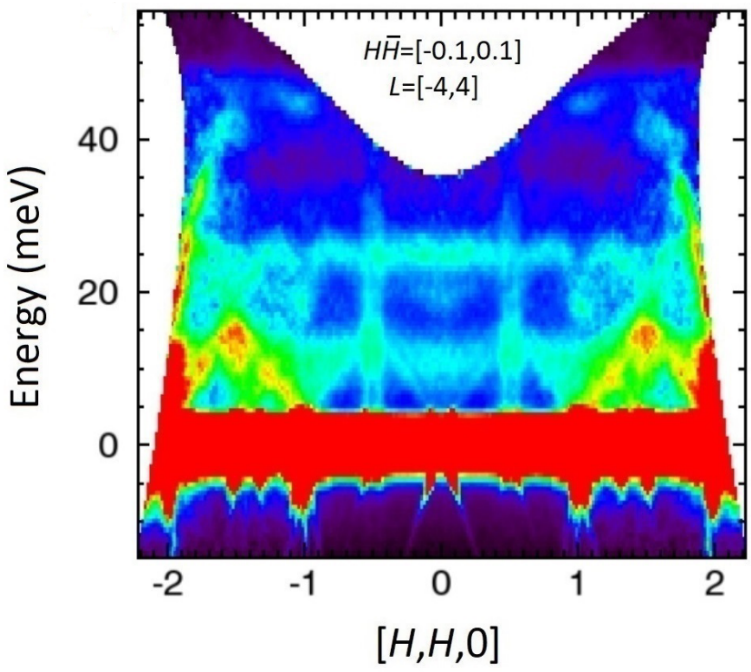

Figure 6.2: Inelastic neutron scattering spectrum of a $La_{1.6-x}Nd_{0.4}Sr_xCuO_4$ sample ($x = 0.12$). Reprinted from Ref. [31] with permission.

6.2 Exchange effect model

The first model to be tested was the one which included exchange field as a possible source of the dichroism observed in the experiment. To check the applicability of this model, 30 T, 50 T and 100 T were tried as possible values of the effective exchange field, without an external field included. The corresponding results are shown on Figure 6.3a.

The initial results resemble the experimental spectrum. However, the similarity vanishes when the external magnetic field is added. Values from -6 to 6 T were tried to produce the graph on Figure 6.3b.

Energy level diagram was also produced during the modeling. Because of the exchange field, the groundstate multiplet is split into 10 distinct levels for all the possible values of J. Many low-lying excitations lead to high temperature sensitivity of the spectrum, because they are quickly populated with the increase in temperature.

It can clearly be seen that the spectrum changes significantly with different values of the magnetic field, contradictory to the results of the experiment.

Therefore, the exchange effect cannot be a sole source of the observed dichroism.

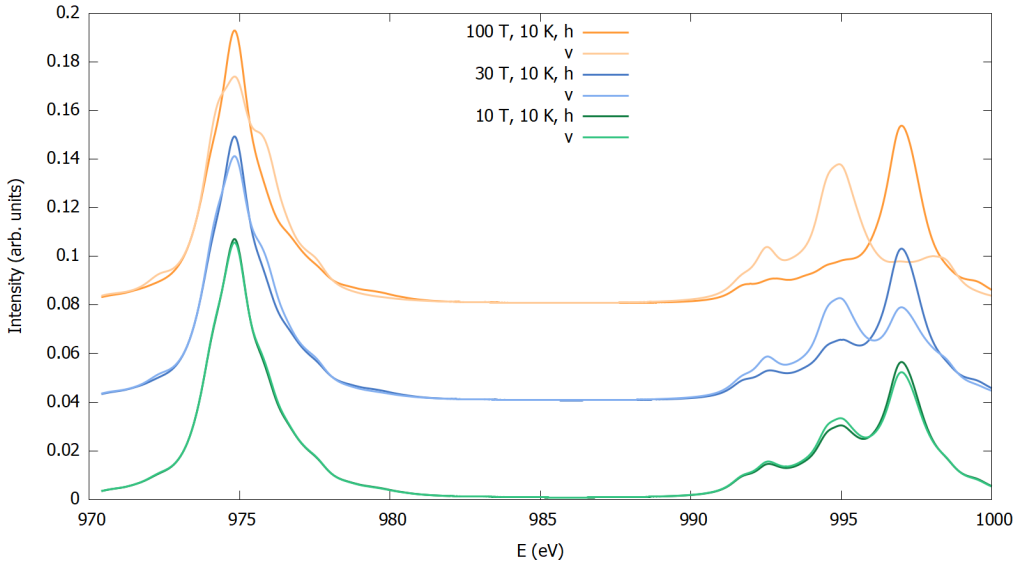

(a) Spectra of an ion with exchange field

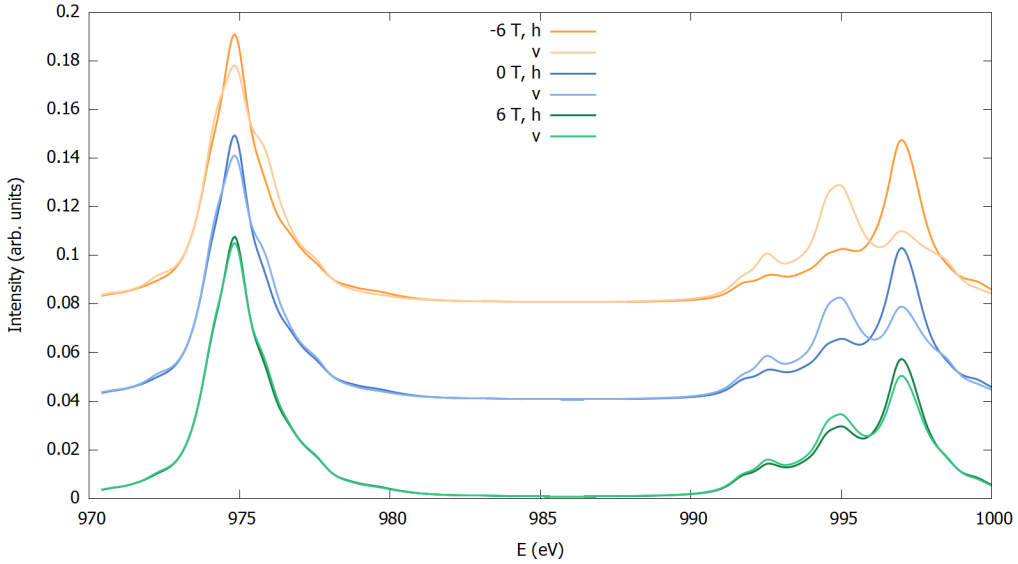

(b) Spectra of an ion with exchange field and magnetic field

Figure 6.3: Spectra of a Nd^{3+} ion with effective exchange field: (a) of the values of 10, 30 and 100 T, (b) of 30 T with parallel (6 T), antiparallel (-6 T) and absent (0 T) external magnetic field. In both cases, v denotes the orientation, parallel to the exchange field direction, whereas h corresponds to the perpendicular direction.

6.3 C_{4v} crystal field model from literature

The second model in the study included a crystal field term as a source of linear dichroism. Several sets of crystal field parameters were tried, starting from the values extracted by infrared transmission spectroscopy in [32]. The first set, labeled as "teor", was calculated from DFT model. The second set, labeled as "fit", was constructed to fit the infrared spectra. Remarkably, four of five parameters have comparable values, while the $B_{4,0}$ parameters differ in sign.

Using these values, the XAS was simulated, and the plots produced are displayed on Figure 6.4. The general look and the temperature-dependent behaviour of the spectra repeat those of the experimental results.

Both of these models result in quite comparable spectra. If an external magnetic field is imposed, linear dichroism is preserved and the spectra look unchanged. The difference between these models becomes noticeable when their temperature dependence is investigated (Figure 6.5):

The cause of this difference is an additional energy level present in the "fit" model at approximately 8 meV. When the temperature increases, this level is getting populated with electrons much faster than the 16 meV level in the "teor" model. The occupation distributions are pictured on a Figure 6.6.

If the individual contributions are investigated, it can be seen that in both models the spectra of the five individual energy levels are comparable and have the same order. They are provided on the Figure 6.7.

If compared to the experiment (see Figure 6.1), however, it can be observed that the groundstate spectrum of the model does not represent the experimental spectrum for 10 K. Instead, the experimental spectrum is closer to the spectrum of the third of five levels. This leads to two possible conclusions:

- The third energy level from the model is actually the groundstate in the experiment. It means that the first (lowest) and the second energy level from the model would be the excited states in the experiment. Thus, the one-electron energies must have a different order.

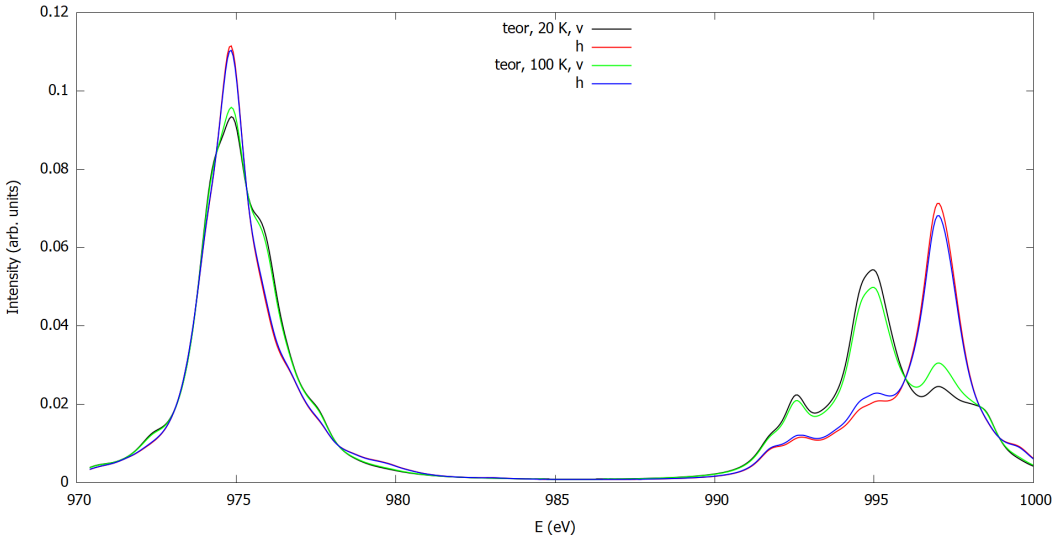

(a) "teor" model

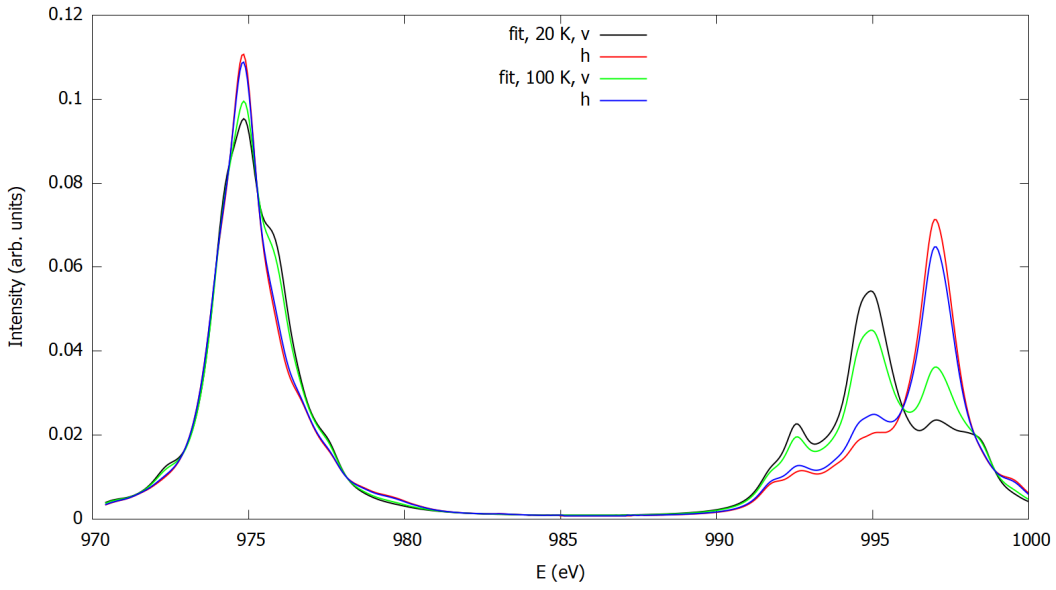

(b) "fit" model

Figure 6.4: The x-ray absorption spectra created using the models "teor" and "fit" from Ref. [32]. Noticeably, the second and third M_4 peaks are substantially different from the experimentally observed. "v" denotes vertical polarization (i.e. parallel to the c axis of a crystal, black and green lines) and "h" denotes horizontal (parallel to the a or b axis, red and blue lines).

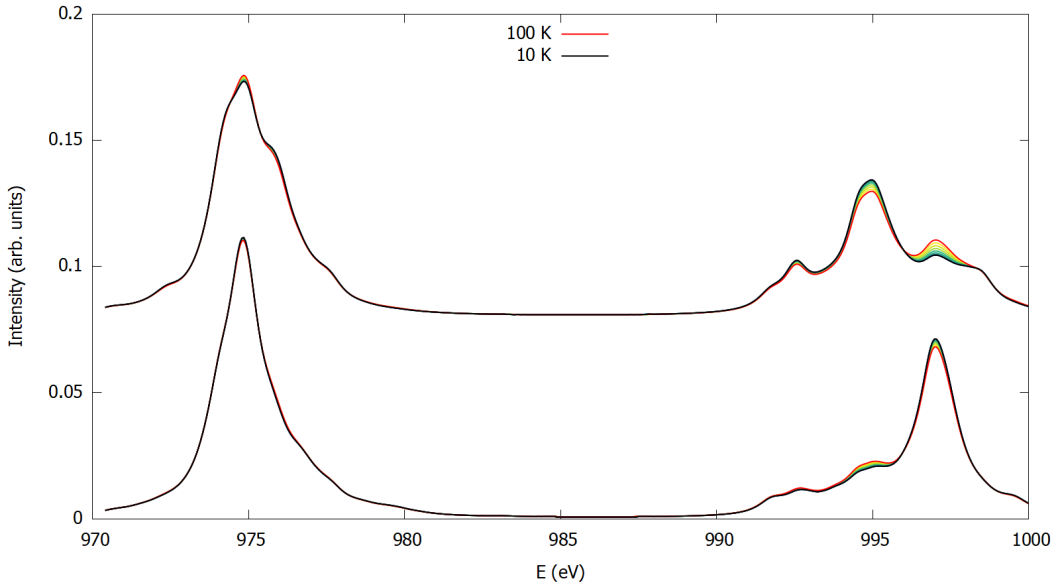

(a) "teor" model

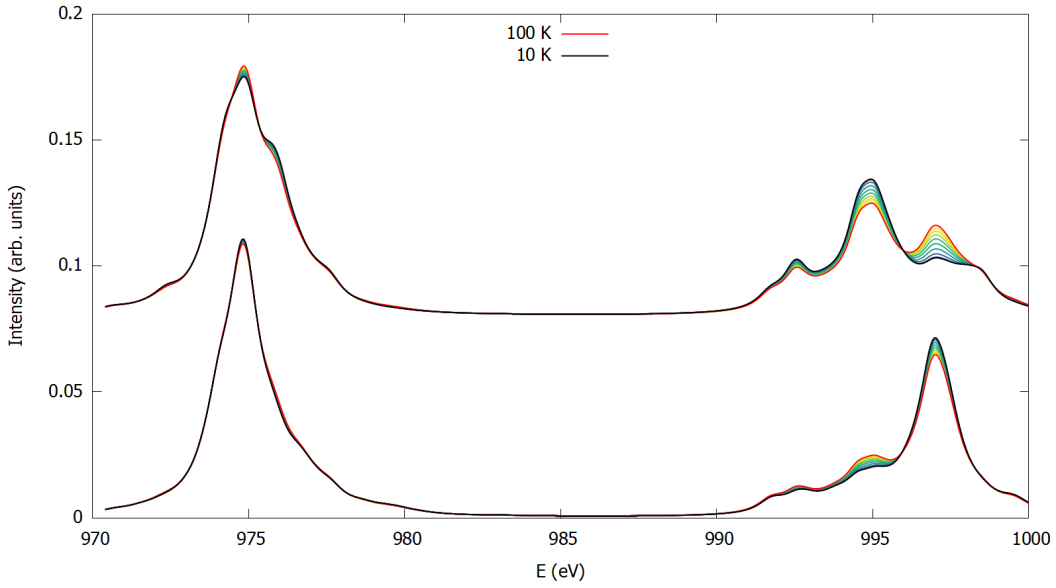

(b) "fit" model

Figure 6.5: Temperature dependence of the x-ray absorption spectra of the models "teor" and "fit" from Ref. [32]. For each of the two plots, top and bottom lines correspond to $\epsilon \parallel c$ and $\epsilon \perp c$ polarizations.

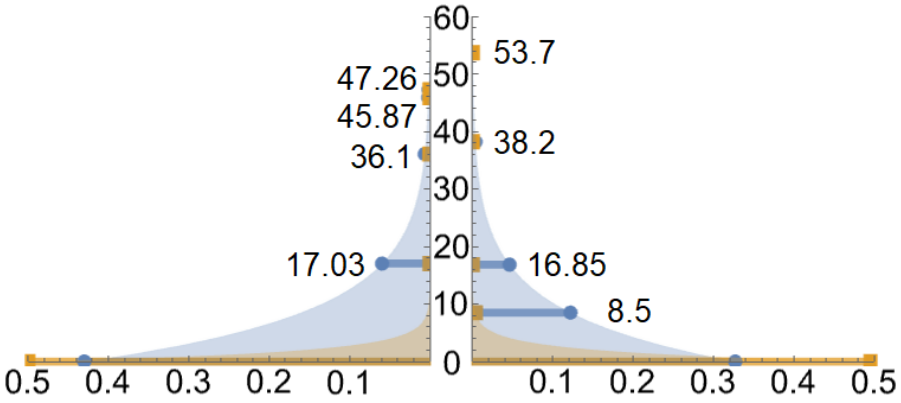

Figure 6.6: Energy levels and their occupations for the "teor" (left) and "fit" (right). Occupation distributions are pictured for the temperatures of 20 K (yellow) and 100 K (blue).

- The energy levels from the model have the same order in the experiment, but have significantly lower energies and are populated already at 10 K. This would mean that the lowest excitations would be observed below 1 meV.

6.4 Inelastic neutron scattering

As mentioned previously, the same material was recently studied using inelastic neutron scattering technique [31]. There, the extracted lowest crystal field excitations were 11, 25 and 45 meV. Quanty gives an opportunity to calculate the lowest eigenenergies simultaneously with the absorption spectra, and uses them to calculate the temperature-dependent spectra. This way, the lowest excitation energies from the modeling can be directly compared to the lowest excitations from the experiment.

The two models proposed by [32] yield the results provided on the Table 6.1. They are somewhat similar, but still not quite close to the energy levels provided by the experiment.

The values of the Wybourne B parameters, suggested by the two models, were fitted using a coordinate descent technique. The "distance" between the modeling and the

teor [32]	fit [32]	exp [31]
17	8.5	11
36	16.85	25
46	38.2	45

Table 6.1: Energies of the three lowest crystal field excitations, meV, proposed by the models in [32] in comparison to the experiment.

experimental values was calculated as Euclidean distance:

$$D = \sqrt{\sum_{i}^{3} (E_{\text{model}} - E_{\text{exp}})^2}$$

The imposed threshold of the fitting accuracy was 3 meV.

For "teor" method, target threshold was reached with 2 iterations (1.8 meV Euclidean distance). In contrast, for "fit" model it took only one iteration to minimize the Euclidean distance to 0.58 meV. If converted to one-electron energies, it can be seen that after the fitting:

- for "teor" model, the order of the energies is preserved, and
- for "fit" model, E_{a2} and E_{b2} are switched but the order of all other energies is preserved.

6.5 Monte-Carlo sampling

While the number of independent crystal field parameters is 5, only 3 energies are defined by the inelastic neutron scattering. It means that for the given 3 energies, there would be a two-dimensional manifold within the 5D parameters space which corresponds to the given energies. It means that to accurately determine the crystal field parameters, an additional

source of information is needed. Moreover, it is unclear whether there are any crystal field excitations with energies lower than 4 meV present in the material. Therefore, there would actually be three manifolds within the parameter space, corresponding to 0, 1 or 2 energy levels, "hidden" under 4 meV.

To explore the possible values of one-electron energies which lead to the same excitation energies and thus localize the manifold described above, disregarding the spectra and physical correctness of the parameters, modified Monte-Carlo sampling was utilized.

The algorithm consists of three parts: generator, calculator, discriminator and optimizer.

Generator generates a set of random numbers which are then used as values of crystal field parameters. Because we are concerned about all of the parameter space, any parameter set can be used as long as it is complete. Here, **generator** creates a list of five random values which then are interpreted as Wybourne $B_{k,q}$ crystal field parameters.

Calculator calculates the lowest excitation energies from the given parameter set. For the sake of simplicity, it is hypothesized that there are no crystal field excitations below 4 meV. Then, the calculated lowest excitations are compared to the experimental values of 11, 25 and 45 meV using the "distance" described in the previous subsection.

Discriminator makes a decision to continue or abort further evaluation based on the calculated "distance". If it is too large, the point is disregarded; if it is less than the optimization threshold, the point is then optimized by the **optimizer**; if it is less than the acceptance threshold, the point is then saved to file.

Optimizer uses a coordinate descent technique to minimize the Euclidean distance between the current point and the experimental values of lowest excitations.

Using this technique, a set of 1000 points was generated. 2D scatter plots were built for each combination of two parameters; they can be found in the Appendix B.

6.6 Absorption spectrum matching

Numerical fitting the values of crystal field parameters presents a multiple factor issue:

- experimental spectrum also includes multiple factors which are not or cannot be taken into account in Quanty;
- experimental spectrum presents the picture where a and b axes are averaged;
- spectra do not depend on crystal field parameters linearly;
- crystal field parameters determine not only the spectra, but also the excitation energies and thus the temperature dependence;
- calculation of a spectrum for a model with a given set of parameters is a computationally expensive task;
- the parameter space is multi-dimensional, requiring at least 5 distinct parameters to be varied.

Because of this, the following study follows a path with minimal need to calculate the spectra, doing so only for a limited number of parameter sets.

The ordering of one-electron energies defines the order in which the energy levels are populated by electrons. Thus, it also defines the order of multielectron wavefunctions with different symmetries and the corresponding absorption spectra contributions. For all the previously investigated models, the E_{eu1} one-electron energy was the lowest of all five. Changing the lowest-energy one-electron state may alter the groundstate of the ion. Therefore, the groundstate spectrum will be different, and thus the temperature-dependent spectrum. The attempts to investigate this dependency are provided below.

The initial attempt was to simply swap the one-electron energy levels with E_{eu1}. Out of four possible combinations, two exhibited a groundstate spectrum which resembled the experimental one: E_{a2u} and E_{b2u}. However, the minimization algorithms utilized show limited success with fitting the three lowest excitations. The Wybourne B parameters,

obtained as a result of the minimization, contain negative $B_{6,0}$ parameter, which is not expected from the system.

The second attempt involves a dataset generated using Monte-Carlo sampling. Starting from the set of 645 points with "distance" less than 5 meV, 185 points were selected with distinct sequence of one-electron energies (if they are sorted from smallest to biggest). For each of the points, the spectra were calculated, and the heights of the three M4 peaks were extracted. Based on these heights, the selection criteria were applied:

- height of the second peak for vertical orientation must be higher than that for the horizontal orientation;
- height of the third peak for vertical orientation must be lower than that for the horizontal orientation;
- height of the third peak for vertical orientation must be lower than that of the second peak, but not more than 1.5 times;
- height of the second peak for vertical orientation must decrease with the temperature increasing to 100 K.

This resulted in only 10 points. The one-electron energy levels comparison of them does not show any systematic similarities. Moreover, the Wybourne $B_{k,q}$ parameters of those points are not in any way close to "teor" and "fit" models mentioned before. The spectra, however, are surprisingly similar to the experimentally observed ones. One of the spectra can be seen on the Figure 6.8. It corresponds to the following Wybourne $B_{k,q}$ parameters:

$$B_{2,0} = -379.4\,\text{meV},\ B_{4,0} = -590.3\,\text{meV},\ B_{4,\pm4} = -7.7\,\text{meV},$$
$$B_{6,0} = -156.6\,\text{meV},\ B_{6,\pm4} = -165\,\text{meV}$$

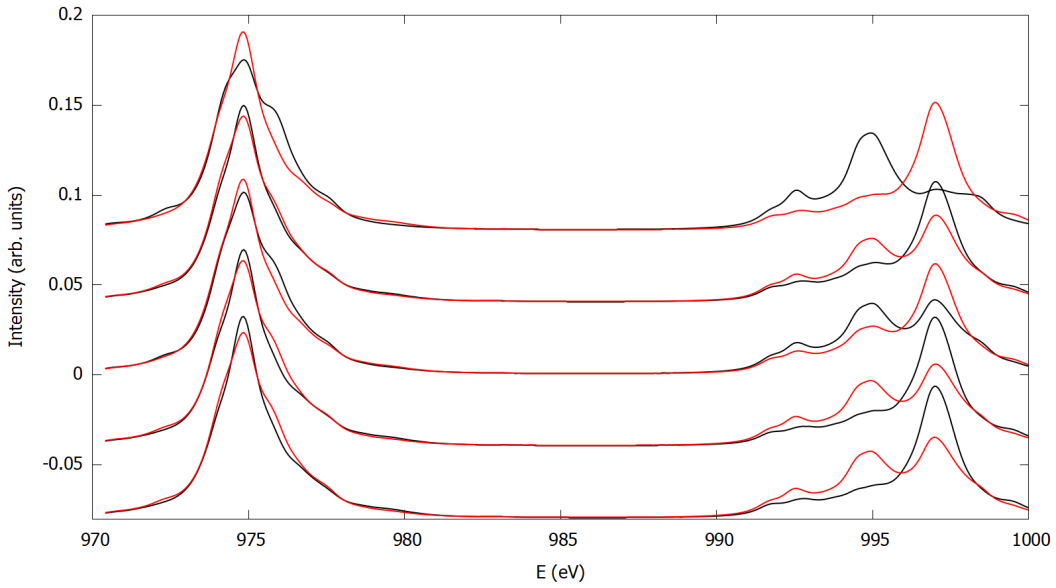

Figure 6.7: Absorption spectra of the lowest eigenstates of the system with "teor" and "fit" parameters. Black line corresponds to $\epsilon \parallel c$ polarization, red line – to $\epsilon \perp c$. Spectra are ordered from top to bottom, where the topmost spectrum corresponds to a lowest energy state. For the zero temperature, the absorption spectrum would be identical to the spectrum of a groundstate; for a non-zero temperature, the absorption spectrum would correspond to a weighted average of the presented spectra. The temperature dependence of the final spectrum for low temperatures would mostly be defined by the spectra of the two or three lowest eigenstates. For example, when the temperature increases, the decrease of the second M4 peak and the increase of the third for the vertical polarization on Figures 6.5a and 6.5b.

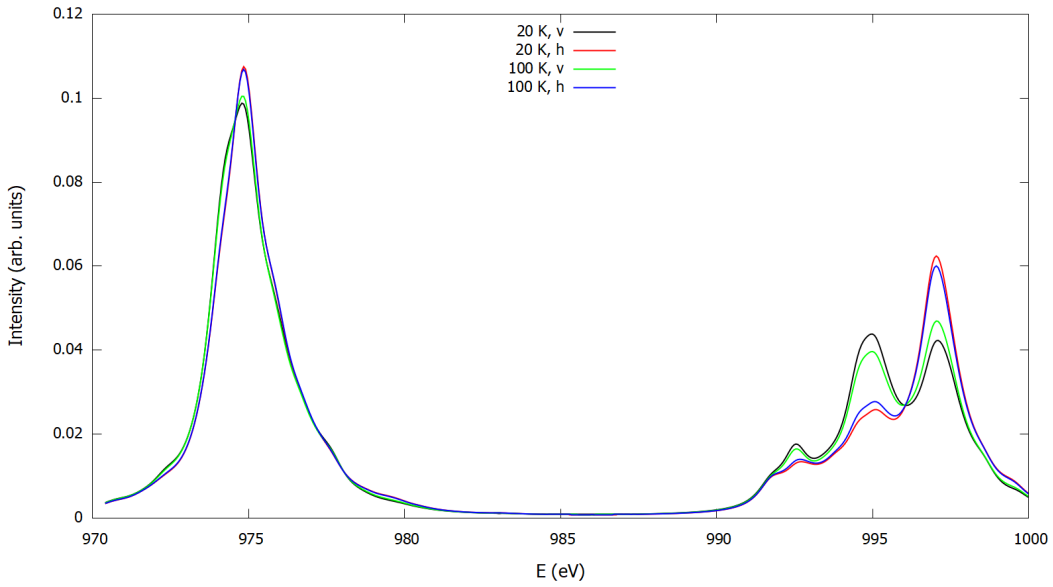

Figure 6.8: X-ray absorption spectrum for a model with C_{4v} symmetry. The parameter set was found via Monte-Carlo sampling and is provided at the end of Section 6.6. "v" label corresponds to $\epsilon \parallel c$ polarization, "h" – to $\epsilon \perp c$ polarization. Simulated spectra are shown for the temperatures of 20 and 100 K.

6.7 C_{2v} crystal field model

C_{2v} picture of the crystal field is a next step after considering C_{4v} symmetry. The LTT and LTO phases of Nd-LSCO, as mentioned in Chapter 2, are characterized by lattice distortion in the form of rotation of CuO_6 octahedra. This correspondingly changes the local symmetry of Neodymium ion, eliminating four-fold vertical axis and thus introducing further symmetry breaking from C_{4v} to C_{2v}. The number of one-electron energies jumps from 6 to 10 due to the splitting of $e1u$ and $e2u$ levels. By introducing C_{2v} field as a splitting of one-electron energies, derived from "teor" and "fit" models, following results were produced.

Lowest excitation energies were matched to 11, 25 and 45 meV using Monte-Carlo sampling and subsequent coordinate descent minimization. 40 parameter sets were generated for both models. Each of those sets was used for modeling the x-ray absorption spectrum.

For "fit" model, the first point found already matched the experimental spectrum. The modeled spectrum is pictured on Figure 6.9. The cause of this matching is the altered energy levels. More precisely, the order of energy levels with particular symmetries is changed, resulting in a groundstate spectrum and first excited level spectra as pictured on Figure 6.10.

(meV)	$B_{2,0}$	$B_{2,\pm2}$	$B_{4,0}$	$B_{4,\pm2}$	$B_{4,\pm4}$	$B_{6,0}$	$B_{6,\pm2}$	$B_{6,\pm4}$	$B_{6,\pm6}$
"fit" [32]	188		-107		-24.8	46		113	
this work	188	28.5	-107	-57.2	-24.8	46	-2	113	51.6

Table 6.2: Wybourne $B_{k,q}$ parameters of the crystal field used in the modeling.

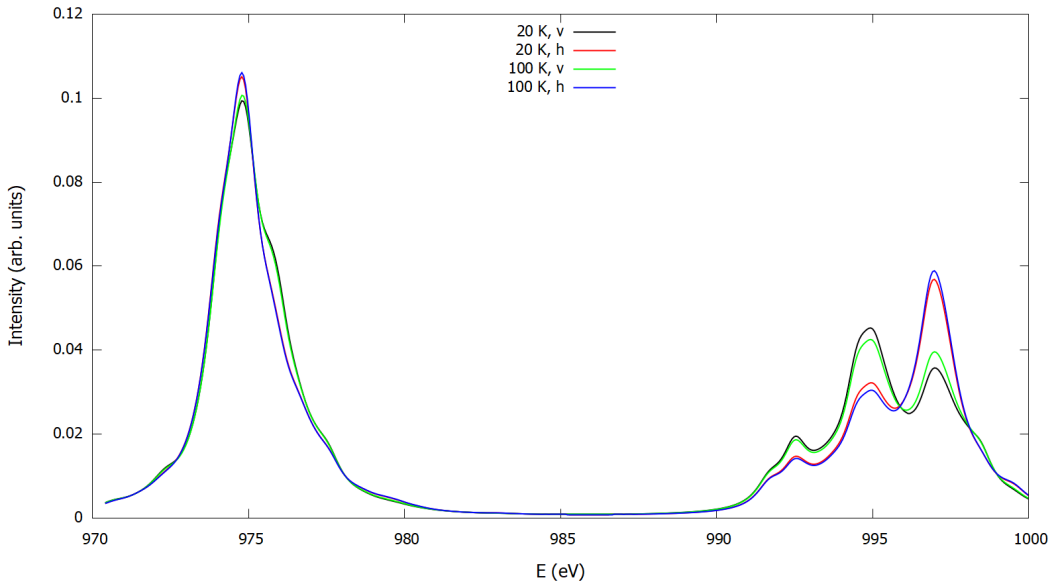

Figure 6.9: X-ray absorption spectrum for a model with C_{2v} symmetry. The parameter set was found via Monte-Carlo sampling and is provided at the end of Section 6.7. "v" label corresponds to $\epsilon \parallel c$ polarization, "h" – to $\epsilon \parallel b$ polarization.. Simulated spectra are shown for the temperatures of 20 and 100 K.

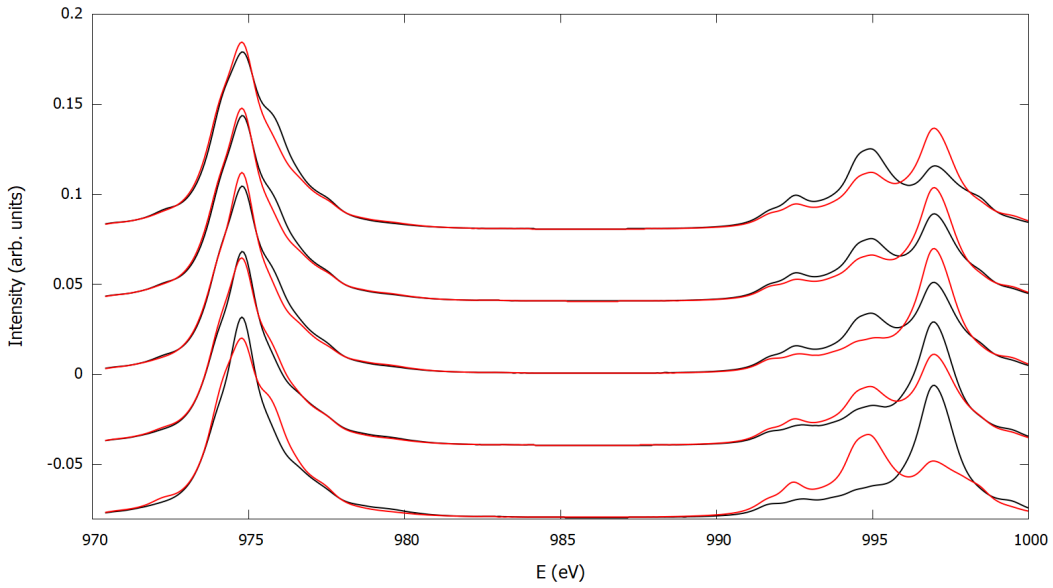

Figure 6.10: X-ray absorption spectra of the five lowest energy levels of a particular parameter set for a model with C_{2v} symmetry, found via Monte-Carlo sampling (Table 6.2). Black lines correspond to $\epsilon \parallel c$ polarization, red lines – to $\epsilon \parallel b$. Spectra are ordered from top to bottom, where the topmost spectrum corresponds to a lowest energy state. The similarity between the spectra of the first two energy levels (compared to 6.7) makes the temperature dependence much more subtle.

6.8 Scattering temperature dependence

The results of the modeling proved C_{2v} crystal field to be consistent with x-ray absorption and inelastic neutron scattering experiments. To investigate the (001) peak scattering intensity, the scattering spectra were reconstructed according to Equation 3.6.

In Figure 6.11a, we show simulated single-ion x-ray absorption spectra at 20 K for an atom in one layer of Nd-LSCO, using crystal field splitting parameters from Table 6.2. This spectra shows a noticeable difference between a and b axes resulting from the C_{2v} crystal field. The resulting (001) peak scattering intensity deduced from the same calculations using Equation 3.6 is shown in Figure 6.11b. Notably, these calculations show that scattering is more prominent at the M_4 absorption edge than at the M_5 edge.

To explore the temperature dependence of the (001) peak, we calculated both the XAS and the (001) peak scattering intensity as a function of temperature resulting from the thermal excitation of crystal field excited states of Nd. Figure 6.12 shows the (001) peak intensity as a function of energy a various temperatures showing the calculated scattering intensity decreases with increasing temperature. This effect is further captured in Figure 6.13a, which shows the (001) peak scattering intensity at selected fixed photon energies as a function of temperature.

A principle conclusion of this work is that, over this temperature range, single-ion effects resulting from the thermal excitation of crystal field excited states can cause a significant temperature dependence to the (001) peak intensity, beyond that resulting from structural distortions in the material.

However, this calculated temperature dependence contrasts with the experimentally observed temperature dependence of Nd^{3+} edge, which exhibits increase in intensity with increasing temperature and a peak at approximately 70 K (Figure 6.13b), as opposed to the decrease in intensity with increasing temperature seen in the calculated temperature dependence.

To explore whether this discrepancy results from the choice of C_{2v} crystal field parameters, an array of 100 different was generated via the Monte-Carlo sampling, and for each of them polarization dependent XAS and the (001) peak temperature dependence were

calculated as a function of temperature.

All parameter sets used in this simulation demonstrate qualitatively identical behaviour: with an increase in temperature, the scattering decreases for the whole displayed range of energies, in contrast with the experimentally observed temperature dependence.

It is clear that the scattering temperature dependence depends on crystal field parameters. For an increase in scattering, an increase in difference between σ_{xx} and σ_{yy} is required. This would be possible if the first or the second excited state of the Nd^{3+} ion would have higher value of $|\sigma_{xx} - \sigma_{yy}|^2$ than the groundstate. It remains unclear whether this is possible for some other realistic values of C_{2v} crystal field parameters that have not yet been sampled.

Further investigation is required to explore the crystal field parameters which may alter the temperature dependence. Crystal field parameters may be easily tweaked, but additional time is required because of the significant time consumption of the spectrum calculation. Additional work will also need to address the magnetic field dependence of the scattering spectrum, observed in the measured spectra on a Figure 6.13b. While the current model is only weakly sensitive to magnetic field, reintroducing an exchange field to the model may increase this sensitivity and alter the scattering temperature dependence.

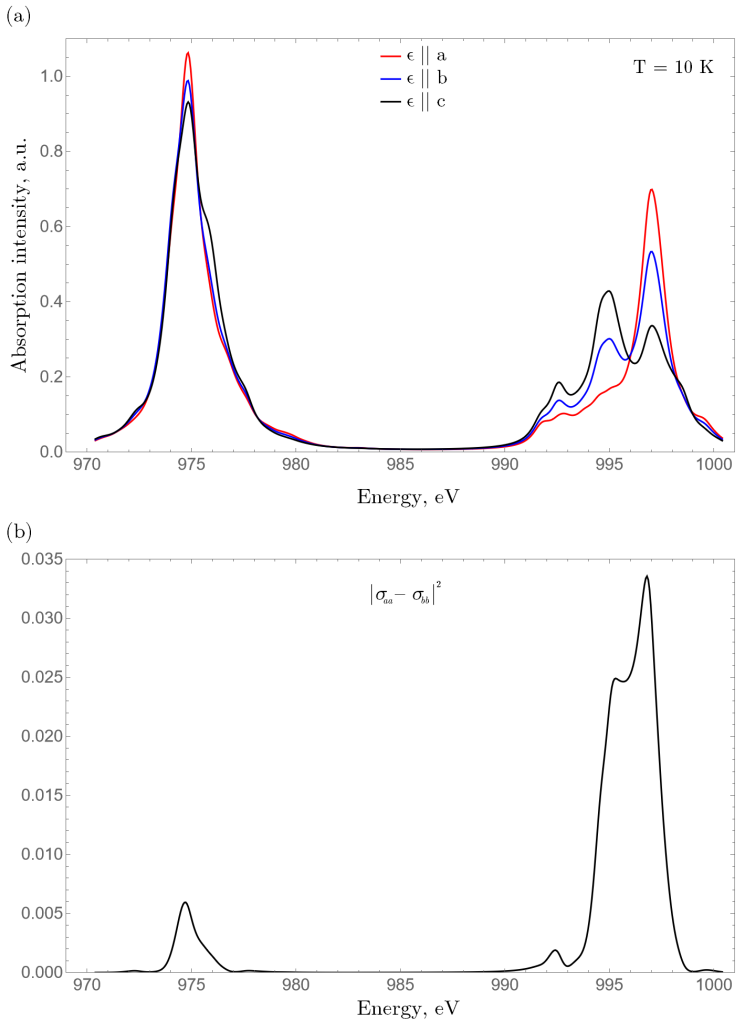

Figure 6.11: (a) x-ray absorption spectra of a single Nd^{3+} ion for the polarization vectors which are parallel to the crystallographic axes. The difference between a and b directions is manifested because of the C_{2v} symmetry of the crystal field. Experimentally, the absorption in perpendicular polarization would correspond to an average between a and b spectra. (b) Squared absolute value of the difference between a and b conductivity. Difference between a and b scattering tensor terms (and thus the scattering intensity) has almost the same shape, because the x-ray energy change is less than 3% over the displayed interval.

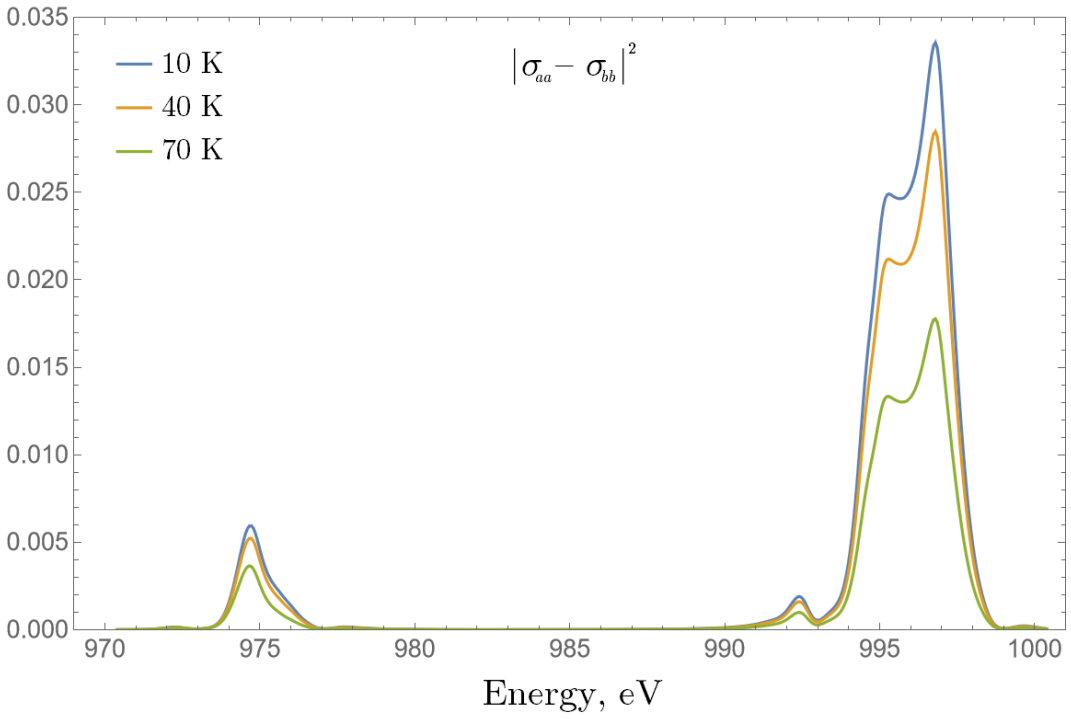

Figure 6.12: Squared absolute value of the difference between a and b conductivity, plotted for three different temperatures with respect to energy. When the temperature increases, the difference between the a and b directions decreases.

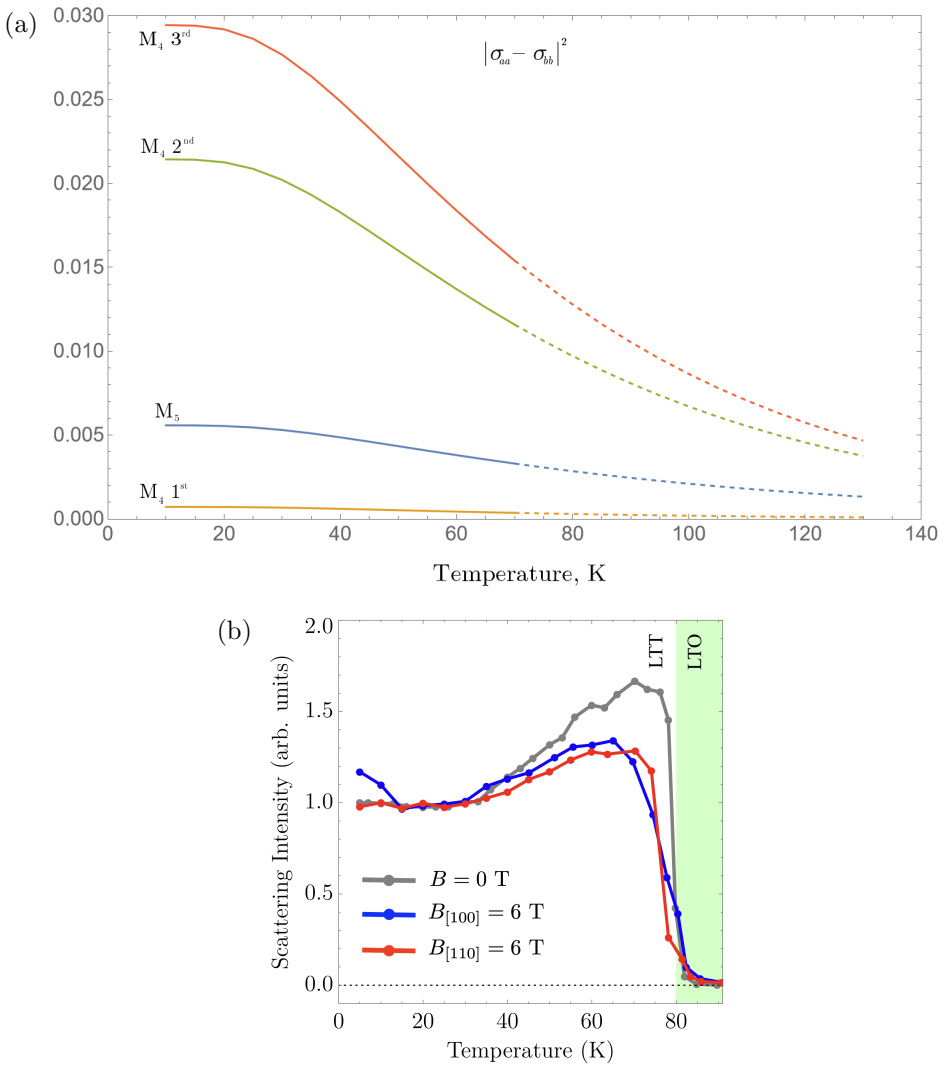

Figure 6.13: (a) Squared absolute value of the difference between a and b conductivity, plotted for the energies of M_4 (994, 996 and 998 eV correspondingly) and M_5 (976 eV) absorption peaks with respect to temperature. The model does not include the LTT to LTO phase transition which happens around 70 K. Thus, the values plotted for the temperatures higher than 70 K are to be viewed only as a hypothetical extrapolation. (b) Temperature dependence of (001) Bragg peak intensities for Nd^{3+} absorption edge in LNSCO crystals (same as Figure 1.1b). Reproduced for convenience. It can be seen that the modelled temperature dependence contrasts with the experimentally observed one.

Chapter 7

Conclusions

The purpose for this work was to explore the cause of the anomalous temperature dependence of the (001) scattering peak at the Nd^{3+} M edge in Nd-doped LSCO. It was hypothesized that this dependence may arise from single-ion phenomena rather from the crystal lattice distortions. To test this hypothesis, we analyzed the temperature and polarization dependence of x-ray absorption spectra of the same system. The analysis was done by building a two-shell model in a dedicated modeling software using the approach of crystal field theory.

We found that the temperature-dependent excitation into low-energy crystal field states results in significant temperature dependence to the single-ion scattering tensor, and thus to the atomic scattering form factor at the Nd^{3+} M edge. This contributes to the temperature dependence of the (001) peak scattering intensity of a crystal lattice, in addition to any lattice-induced rotational symmetry breaking.

We established that realistic crystal field parameters for a field with C_{2v} symmetry capture both the temperature dependence and polarization dependence of the measured x-ray absorption spectra. Moreover, they are consistent with crystal field excitations measured by inelastic neutron scattering.

However, the model based on realistic C_{2v} crystal field parameters, while being consistent with x-ray absorption spectrum and inelastic neutron scattering, does not capture the

correct temperature dependence of the (001) scattering peak. The experimental temperature dependence demonstrates an increase in intensity with increasing temperature and a peak at approximately 70 K; in contrast, simulated scattering exhibits steady decrease in intensity.

To check if this behaviour arises only from a specific chosen set of crystal field parameters, 100 different sets were generated, and the temperature dependence of x-ray absorption and (001) scattering peak intensity were calculated for all of them. The results show that all generated sets lead to the same behaviour: with an increase in temperature, the difference between a and b directions decreases, leading to a decrease in single-ion scattering intensity.

The observed increase in (001) scattering intensity would be manifested if the difference between xx and yy components of a single-ion scattering tensor was larger for the excited states than for the groundstate. It is unclear whether such situation is possible for some values of the C_{2v} crystal field parameters which were not tested in the current work.

Therefore, further work will be dedicated to identify if refinement of the crystal field parameters can realize this possibility. Additionally, the magnetic field dependence of the scattering spectrum has to be addressed. It is possible that the inclusion of the exchange interaction in addition to crystal field would correspond to this dependence.

Letters of Copyright Permissions

CCC Marketplace™

This is a License Agreement between Anton Lutsenko ("User") and Copyright Clearance Center, Inc. ("CCC") on behalf of the Rightsholder identified in the order details below. The license consists of the order details, the CCC Terms and Conditions below, and any Rightsholder Terms and Conditions which are included below.

All payments must be made in full to CCC in accordance with the CCC Terms and Conditions below.

Order Date	02-Jun-2022	Type of Use	Republish in a thesis/dissertation
Order License ID	1228195-1		
ISSN	0953-8984	Publisher	IOP Publishing
		Portion	Chart/graph/table/figure

LICENSED CONTENT

Publication Title	Journal of Physics	Country	United Kingdom of Great Britain and Northern Ireland
Author/Editor	Institute of Physics (Great Britain)	Rightsholder	IOP Publishing, Ltd
Date	01/01/1989	Publication Type	Journal
Language	English		

REQUEST DETAILS

Portion Type	Chart/graph/table/figure	Distribution	Canada
Number of charts / graphs / tables / figures requested	1	Translation	Original language of publication
Format (select all that apply)	Electronic	Copies for the disabled?	No
		Minor editing privileges?	No
Who will republish the content?	Academic institution	Incidental promotional use?	No
Duration of Use	Life of current edition	Currency	CAD
Lifetime Unit Quantity	Up to 499		
Rights Requested	Main product		

NEW WORK DETAILS

Title	Modeling the X-ray absorption of Neodymium ions in cuprate superconductors	Institution name	University of Waterloo
		Expected presentation date	2022-06-27
Instructor name	David Hawthorn		

ADDITIONAL DETAILS

Order reference number	N/A	The requesting person / organization to appear on the license	Anton Lutsenko

REUSE CONTENT DETAILS

Title, description or numeric reference of the portion(s)	Figure 6. Phase diagram of Nd-LSCO.	Title of the article/chapter the portion is from	Fermi surface reconstruction in high-Tc superconductors
Editor of portion(s)	N/A	Author of portion(s)	Institute of Physics (Great Britain)
Volume of serial or monograph	N/A		

Page or page range of portion	1	**Issue, if republishing an article from a serial**	N/A
		Publication date of portion	2009-03-31

RIGHTSHOLDER TERMS AND CONDITIONS

These special terms and conditions are in addition to the standard terms and conditions for CCC's Republication Service and, together with those standard terms and conditions, govern the use of the Works. As the User you will make all reasonable efforts to contact the author(s) of the article which the Work is to be reused from, to seek consent for your intended use. Contacting one author who is acting expressly as authorised agent for their co-author(s) is acceptable. User will reproduce the following wording prominently alongside the Work: the source of the Work, including author, article title, title of journal, volume number, issue number (if relevant), page range (or first page if this is the only information available) and date of first publication; and a link back to the article (via DOI); and if practicable, and IN ALL CASES for new works published under any of the Creative Commons licences, the words "© IOP Publishing. Reproduced with permission. All rights reserved" Without the express permission of the author(s) and the Rightsholder of the article from which the Work is to be reused, User shall not use it in any way which, in the opinion of the Rightsholder, could: (i) distort or alter the author(s)' original intention(s) and meaning; (ii) be prejudicial to the honour or reputation of the author(s); and/or (iii) imply endorsement by the author(s) and/or the Rightsholder. This licence does not apply to any article which is credited to another source and which does not have the copyright line '© IOP Publishing Ltd'. User must check the copyright line of the article from which the Work is to be reused to check that IOP Publishing Ltd has all the necessary rights to be able to grant permission. User is solely responsible for identifying and obtaining separate licences and permissions from the copyright owner for reuse of any such third party material/figures which the Rightsholder is not the copyright owner of. The Rightsholder shall not reimburse any fees which User pays for a republication license for such third party content. This licence does not apply to any material/figure which is credited to another source in the Rightsholder's publication or has been obtained from a third party. User must check the Version of Record of the article from which the Work is to be reused, to check whether any of the material in the Work is third party material. Third party citations and/or copyright notices and/or permissions statements may not be included in any other version of the article from which the Work is to be reused and so cannot be relied upon by the User. User is solely responsible for identifying and obtaining separate licences and permissions from the copyright owner for reuse of any such third party material/figures where the Rightsholder is not the copyright owner. The Rightsholder shall not reimburse any fees which User pays for a republication license for such third party content. User and CCC acknowledge that the Rightsholder may, from time to time, make changes or additions to these special terms and conditions without express notification, provided that these shall not apply to permissions already secured and paid for by User prior to such change or addition. User acknowledges that the Rightsholder (which includes companies within its group and third parties for whom it publishes its titles) may make use of personal data collected through the service in the course of their business. If User is the author of the Work, User may automatically have the right to reuse it under the rights granted back when User transferred the copyright in the article to the Rightsholder. User should check the copyright form and the relevant author rights policy to check whether permission is required. If User is the author of the Work and does require permission for proposed reuse of the Work, User should select 'Author of requested content' as the Requestor Type. The Rightsholder shall not reimburse any fees which User pays for a republication license. If User is the author of the article which User wishes to reuse in User's thesis or dissertation, the republication licence covers the right to include the Version of Record of the article, provided it is not then shared or deposited online. User must include citation details. Where User wishes to share their thesis or dissertation online, they should remove the Version of Record before uploading it. User may include a Preprint or the Accepted Manuscript (after the embargo period) in the online version of the thesis or dissertation, provided they do so in accordance with the Rightsholder's policies on sharing Preprints or Accepted Manuscripts. User may need to obtain separate permission for any third party content included within the article. User must check this with the copyright owner of such third party content. Any online or commercial use of User's thesis or dissertation containing the article, including publication via ProQuest, would need to be expressly notified in writing to the Rightsholder at the time of request and would require separate written permission from the Rightsholder. As well as CCC, the Rightsholder shall have the right to bring any legal action that it deems necessary to enforce its rights should it consider that the Work infringes those rights in any way. For content reuse requests that qualify for permission under the STM Permissions Guidelines, which may be updated from time to time, the STM Permissions Guidelines supplement the terms and conditions contained in this license.

Marketplace Order General Terms and Conditions

The following terms and conditions ("General Terms"), together with any applicable Publisher Terms and Conditions, govern User's use of Works pursuant to the Licenses granted by Copyright Clearance Center, Inc. ("CCC") on behalf of the applicable Rightsholders of such Works through CCC's applicable Marketplace transactional licensing services (each, a "Service").

1) **Definitions.** For purposes of these General Terms, the following definitions apply:

"License" is the licensed use the User obtains via the Marketplace platform in a particular licensing transaction, as set forth in the Order Confirmation.

"Order Confirmation" is the confirmation CCC provides to the User at the conclusion of each Marketplace transaction. "Order Confirmation Terms" are additional terms set forth on specific Order Confirmations not set forth in the General Terms that can include terms applicable to a particular CCC transactional licensing service and/or any Rightsholder-specific terms.

"Rightsholder(s)" are the holders of copyright rights in the Works for which a User obtains licenses via the Marketplace platform, which are displayed on specific Order Confirmations.

"Terms" means the terms and conditions set forth in these General Terms and any additional Order Confirmation Terms collectively.

"User" or "you" is the person or entity making the use granted under the relevant License. Where the person accepting the Terms on behalf of a User is a freelancer or other third party who the User authorized to accept the General Terms on the User's behalf, such person shall be deemed jointly a User for purposes of such Terms.

"Work(s)" are the copyright protected works described in relevant Order Confirmations.

2) **Description of Service.** CCC's Marketplace enables Users to obtain Licenses to use one or more Works in accordance with all relevant Terms. CCC grants Licenses as an agent on behalf of the copyright rightsholder identified in the relevant Order Confirmation.

3) **Applicability of Terms.** The Terms govern User's use of Works in connection with the relevant License. In the event of any conflict between General Terms and Order Confirmation Terms, the latter shall govern. User acknowledges that Rightsholders have complete discretion whether to grant any permission, and whether to place any limitations on any grant, and that CCC has no right to supersede or to modify any such discretionary act by a Rightsholder.

4) **Representations; Acceptance.** By using the Service, User represents and warrants that User has been duly authorized by the User to accept, and hereby does accept, all Terms.

5) **Scope of License; Limitations and Obligations.** All Works and all rights therein, including copyright rights, remain the sole and exclusive property of the Rightsholder. The License provides only those rights expressly set forth in the terms and conveys no other rights in any Works

6) **General Payment Terms.** User may pay at time of checkout by credit card or choose to be invoiced. If the User chooses to be invoiced, the User shall: (i) remit payments in the manner identified on specific invoices, (ii) unless otherwise specifically stated in an Order Confirmation or separate written agreement, Users shall remit payments upon receipt of the relevant invoice from CCC, either by delivery or notification of availability of the invoice via the Marketplace platform, and (iii) if the User does not pay the invoice within 30 days of receipt, the User may incur a service charge of 1.5% per month or the maximum rate allowed by applicable law, whichever is less. While User may exercise the rights in the License immediately upon receiving the Order Confirmation, the License is automatically revoked and is null and void, as if it had never been issued, if CCC does not receive complete payment on a timely basis.

7) **General Limits on Use.** Unless otherwise provided in the Order Confirmation, any grant of rights to User (i) involves only the rights set forth in the Terms and does not include subsequent or additional uses, (ii) is non-exclusive and non-transferable, and (iii) is subject to any and all limitations and restrictions (such as, but not limited to, limitations on duration of use or circulation) included in the Terms. Upon completion of the licensed use as set forth in the Order Confirmation, User shall either secure a new permission for further use of the Work(s) or immediately cease any new use of the Work(s) and shall render inaccessible (such as by deleting or by removing or severing links or other locators) any further copies of the Work. User may only make alterations to the Work if and as expressly set forth in the Order Confirmation. No Work may be used in any way that is defamatory, violates the rights of third parties (including such third parties' rights of copyright, privacy, publicity, or other tangible or intangible property), or is otherwise illegal, sexually explicit, or obscene. In addition, User may not conjoin a Work with any other material that may result in damage to the reputation of the Rightsholder. User agrees to inform CCC if it becomes aware of any infringement of any rights in a Work and to cooperate with any reasonable request of CCC or the Rightsholder in connection therewith.

8) **Third Party Materials.** In the event that the material for which a License is sought includes third party materials (such as photographs, illustrations, graphs, inserts and similar materials) that are identified in such material as having been used by permission (or a similar indicator), User is responsible for identifying, and seeking separate licenses (under this Service, if available, or otherwise) for any of such third party materials; without a separate license, User may not use such third party materials via the License.

9) **Copyright Notice.** Use of proper copyright notice for a Work is required as a condition of any License granted under the Service. Unless otherwise provided in the Order Confirmation, a proper copyright notice will read substantially as follows: "Used with permission of [Rightsholder's name], from [Work's title, author, volume, edition number and year of copyright]; permission conveyed through Copyright Clearance Center, Inc." Such notice must be provided in a reasonably legible font size and must be placed either on a cover page or in another location that any person, upon gaining access to the material which is the subject of a permission, shall see, or in the case of republication Licenses, immediately adjacent to the Work as used (for example, as part of a by-line or footnote) or in the place where substantially all other credits or notices for the

new work containing the republished Work are located. Failure to include the required notice results in loss to the Rightsholder and CCC, and the User shall be liable to pay liquidated damages for each such failure equal to twice the use fee specified in the Order Confirmation, in addition to the use fee itself and any other fees and charges specified.

10) **Indemnity.** User hereby indemnifies and agrees to defend the Rightsholder and CCC, and their respective employees and directors, against all claims, liability, damages, costs, and expenses, including legal fees and expenses, arising out of any use of a Work beyond the scope of the rights granted herein and in the Order Confirmation, or any use of a Work which has been altered in any unauthorized way by User, including claims of defamation or infringement of rights of copyright, publicity, privacy, or other tangible or intangible property.

11) **Limitation of Liability.** UNDER NO CIRCUMSTANCES WILL CCC OR THE RIGHTSHOLDER BE LIABLE FOR ANY DIRECT, INDIRECT, CONSEQUENTIAL, OR INCIDENTAL DAMAGES (INCLUDING WITHOUT LIMITATION DAMAGES FOR LOSS OF BUSINESS PROFITS OR INFORMATION, OR FOR BUSINESS INTERRUPTION) ARISING OUT OF THE USE OR INABILITY TO USE A WORK, EVEN IF ONE OR BOTH OF THEM HAS BEEN ADVISED OF THE POSSIBILITY OF SUCH DAMAGES. In any event, the total liability of the Rightsholder and CCC (including their respective employees and directors) shall not exceed the total amount actually paid by User for the relevant License. User assumes full liability for the actions and omissions of its principals, employees, agents, affiliates, successors, and assigns.

12) **Limited Warranties.** THE WORK(S) AND RIGHT(S) ARE PROVIDED "AS IS." CCC HAS THE RIGHT TO GRANT TO USER THE RIGHTS GRANTED IN THE ORDER CONFIRMATION DOCUMENT. CCC AND THE RIGHTSHOLDER DISCLAIM ALL OTHER WARRANTIES RELATING TO THE WORK(S) AND RIGHT(S), EITHER EXPRESS OR IMPLIED, INCLUDING WITHOUT LIMITATION IMPLIED WARRANTIES OF MERCHANTABILITY OR FITNESS FOR A PARTICULAR PURPOSE. ADDITIONAL RIGHTS MAY BE REQUIRED TO USE ILLUSTRATIONS, GRAPHS, PHOTOGRAPHS, ABSTRACTS, INSERTS, OR OTHER PORTIONS OF THE WORK (AS OPPOSED TO THE ENTIRE WORK) IN A MANNER CONTEMPLATED BY USER; USER UNDERSTANDS AND AGREES THAT NEITHER CCC NOR THE RIGHTSHOLDER MAY HAVE SUCH ADDITIONAL RIGHTS TO GRANT.

13) **Effect of Breach.** Any failure by User to pay any amount when due, or any use by User of a Work beyond the scope of the License set forth in the Order Confirmation and/or the Terms, shall be a material breach of such License. Any breach not cured within 10 days of written notice thereof shall result in immediate termination of such License without further notice. Any unauthorized (but licensable) use of a Work that is terminated immediately upon notice thereof may be liquidated by payment of the Rightsholder's ordinary license price therefor; any unauthorized (and unlicensable) use that is not terminated immediately for any reason (including, for example, because materials containing the Work cannot reasonably be recalled) will be subject to all remedies available at law or in equity, but in no event to a payment of less than three times the Rightsholder's ordinary license price for the most closely analogous licensable use plus Rightsholder's and/or CCC's costs and expenses incurred in collecting such payment.

14) **Additional Terms for Specific Products and Services.** If a User is making one of the uses described in this Section 14, the additional terms and conditions apply:

a) ***Print Uses of Academic Course Content and Materials (photocopies for academic coursepacks or classroom handouts).*** For photocopies for academic coursepacks or classroom handouts the following additional terms apply:

i) The copies and anthologies created under this License may be made and assembled by faculty members individually or at their request by on-campus bookstores or copy centers, or by off-campus copy shops and other similar entities.

ii) No License granted shall in any way: (i) include any right by User to create a substantively non-identical copy of the Work or to edit or in any other way modify the Work (except by means of deleting material immediately preceding or following the entire portion of the Work copied) (ii) permit "publishing ventures" where any particular anthology would be systematically marketed at multiple institutions.

iii) Subject to any Publisher Terms (and notwithstanding any apparent contradiction in the Order Confirmation arising from data provided by User), any use authorized under the academic pay-per-use service is limited as follows:

A) any License granted shall apply to only one class (bearing a unique identifier as assigned by the institution, and thereby including all sections or other subparts of the class) at one institution;

B) use is limited to not more than 25% of the text of a book or of the items in a published collection of essays, poems or articles;

C) use is limited to no more than the greater of (a) 25% of the text of an issue of a journal or other periodical or (b) two articles from such an issue;

D) no User may sell or distribute any particular anthology, whether photocopied or electronic, at more than one institution of learning;

E) in the case of a photocopy permission, no materials may be entered into electronic memory by User except

in order to produce an identical copy of a Work before or during the academic term (or analogous period) as to which any particular permission is granted. In the event that User shall choose to retain materials that are the subject of a photocopy permission in electronic memory for purposes of producing identical copies more than one day after such retention (but still within the scope of any permission granted), User must notify CCC of such fact in the applicable permission request and such retention shall constitute one copy actually sold for purposes of calculating permission fees due; and

F) any permission granted shall expire at the end of the class. No permission granted shall in any way include any right by User to create a substantively non-identical copy of the Work or to edit or in any other way modify the Work (except by means of deleting material immediately preceding or following the entire portion of the Work copied).

iv) Books and Records; Right to Audit. As to each permission granted under the academic pay-per-use Service, User shall maintain for at least four full calendar years books and records sufficient for CCC to determine the numbers of copies made by User under such permission. CCC and any representatives it may designate shall have the right to audit such books and records at any time during User's ordinary business hours, upon two days' prior notice. If any such audit shall determine that User shall have underpaid for, or underreported, any photocopies sold or by three percent (3%) or more, then User shall bear all the costs of any such audit; otherwise, CCC shall bear the costs of any such audit. Any amount determined by such audit to have been underpaid by User shall immediately be paid to CCC by User, together with interest thereon at the rate of 10% per annum from the date such amount was originally due. The provisions of this paragraph shall survive the termination of this License for any reason.

b) ***Digital Pay-Per-Uses of Academic Course Content and Materials (e-coursepacks, electronic reserves, learning management systems, academic institution intranets).*** For uses in e-coursepacks, posts in electronic reserves, posts in learning management systems, or posts on academic institution intranets, the following additional terms apply:

i) The pay-per-uses subject to this Section 14(b) include:

A) **Posting e-reserves, course management systems, e-coursepacks for text-based content,** which grants authorizations to import requested material in electronic format, and allows electronic access to this material to members of a designated college or university class, under the direction of an instructor designated by the college or university, accessible only under appropriate electronic controls (e.g., password);

B) **Posting e-reserves, course management systems, e-coursepacks for material consisting of photographs or other still images not embedded in text,** which grants not only the authorizations described in Section 14(b)(i)(A) above, but also the following authorization: to include the requested material in course materials for use consistent with Section 14(b)(i)(A) above, including any necessary resizing, reformatting or modification of the resolution of such requested material (provided that such modification does not alter the underlying editorial content or meaning of the requested material, and provided that the resulting modified content is used solely within the scope of, and in a manner consistent with, the particular authorization described in the Order Confirmation and the Terms), but not including any other form of manipulation, alteration or editing of the requested material;

C) **Posting e-reserves, course management systems, e-coursepacks or other academic distribution for audiovisual content,** which grants not only the authorizations described in Section 14(b)(i)(A) above, but also the following authorizations: (i) to include the requested material in course materials for use consistent with Section 14(b)(i)(A) above; (ii) to display and perform the requested material to such members of such class in the physical classroom or remotely by means of streaming media or other video formats; and (iii) to "clip" or reformat the requested material for purposes of time or content management or ease of delivery, provided that such "clipping" or reformatting does not alter the underlying editorial content or meaning of the requested material and that the resulting material is used solely within the scope of, and in a manner consistent with, the particular authorization described in the Order Confirmation and the Terms. Unless expressly set forth in the relevant Order Conformation, the License does not authorize any other form of manipulation, alteration or editing of the requested material.

ii) Unless expressly set forth in the relevant Order Confirmation, no License granted shall in any way: (i) include any right by User to create a substantively non-identical copy of the Work or to edit or in any other way modify the Work (except by means of deleting material immediately preceding or following the entire portion of the Work copied or, in the case of Works subject to Sections 14(b)(1)(B) or (C) above, as described in such Sections) (ii) permit "publishing ventures" where any particular course materials would be systematically marketed at multiple institutions.

iii) Subject to any further limitations determined in the Rightsholder Terms (and notwithstanding any apparent contradiction in the Order Confirmation arising from data provided by User), any use authorized under the electronic course content pay-per-use service is limited as follows:

A) any License granted shall apply to only one class (bearing a unique identifier as assigned by the institution, and thereby including all sections or other subparts of the class) at one institution;

B) use is limited to not more than 25% of the text of a book or of the items in a published collection of essays, poems or articles;

C) use is limited to not more than the greater of (a) 25% of the text of an issue of a journal or other periodical or (b) two articles from such an issue;

D) no User may sell or distribute any particular materials, whether photocopied or electronic, at more than one institution of learning;

E) electronic access to material which is the subject of an electronic-use permission must be limited by means of electronic password, student identification or other control permitting access solely to students and instructors in the class;

F) User must ensure (through use of an electronic cover page or other appropriate means) that any person, upon gaining electronic access to the material, which is the subject of a permission, shall see:

- a proper copyright notice, identifying the Rightsholder in whose name CCC has granted permission,
- a statement to the effect that such copy was made pursuant to permission,
- a statement identifying the class to which the material applies and notifying the reader that the material has been made available electronically solely for use in the class, and
- a statement to the effect that the material may not be further distributed to any person outside the class, whether by copying or by transmission and whether electronically or in paper form, and User must also ensure that such cover page or other means will print out in the event that the person accessing the material chooses to print out the material or any part thereof.

G) any permission granted shall expire at the end of the class and, absent some other form of authorization, User is thereupon required to delete the applicable material from any electronic storage or to block electronic access to the applicable material.

iv) Uses of separate portions of a Work, even if they are to be included in the same course material or the same university or college class, require separate permissions under the electronic course content pay-per-use Service. Unless otherwise provided in the Order Confirmation, any grant of rights to User is limited to use completed no later than the end of the academic term (or analogous period) as to which any particular permission is granted.

v) Books and Records; Right to Audit. As to each permission granted under the electronic course content Service, User shall maintain for at least four full calendar years books and records sufficient for CCC to determine the numbers of copies made by User under such permission. CCC and any representatives it may designate shall have the right to audit such books and records at any time during User's ordinary business hours, upon two days' prior notice. If any such audit shall determine that User shall have underpaid for, or underreported, any electronic copies used by three percent (3%) or more, then User shall bear all the costs of any such audit; otherwise, CCC shall bear the costs of any such audit. Any amount determined by such audit to have been underpaid by User shall immediately be paid to CCC by User, together with interest thereon at the rate of 10% per annum from the date such amount was originally due. The provisions of this paragraph shall survive the termination of this license for any reason.

c) ***Pay-Per-Use Permissions for Certain Reproductions (Academic photocopies for library reserves and interlibrary loan reporting) (Non-academic internal/external business uses and commercial document delivery).*** The License expressly excludes the uses listed in Section (c)(i)-(v) below (which must be subject to separate license from the applicable Rightsholder) for: academic photocopies for library reserves and interlibrary loan reporting; and non-academic internal/external business uses and commercial document delivery.

i) electronic storage of any reproduction (whether in plain-text, PDF, or any other format) other than on a transitory basis;

ii) the input of Works or reproductions thereof into any computerized database;

iii) reproduction of an entire Work (cover-to-cover copying) except where the Work is a single article;

iv) reproduction for resale to anyone other than a specific customer of User;

v) republication in any different form. Please obtain authorizations for these uses through other CCC services or directly from the rightsholder.

Any license granted is further limited as set forth in any restrictions included in the Order Confirmation and/or in these Terms.

d) ***Electronic Reproductions in Online Environments (Non-Academic-email, intranet, internet and extranet).*** For "electronic reproductions", which generally includes e-mail use (including instant messaging or other electronic transmission to a defined group of recipients) or posting on an intranet, extranet or Intranet site (including any display or performance incidental thereto), the following additional terms apply:

i) Unless otherwise set forth in the Order Confirmation, the License is limited to use completed within 30 days for any use on the Internet, 60 days for any use on an intranet or extranet and one year for any other use, all as measured from the "republication date" as identified in the Order Confirmation, if any, and otherwise from the date of the Order Confirmation.

ii) User may not make or permit any alterations to the Work, unless expressly set forth in the Order Confirmation (after request by User and approval by Rightsholder); provided, however, that a Work consisting of photographs or other still images not embedded in text may, if necessary, be resized, reformatted or have its resolution modified without additional express permission, and a Work consisting of audiovisual content may, if necessary, be "clipped" or reformatted for purposes of time or content management or ease of delivery (provided that any such resizing, reformatting, resolution modification or “clipping” does not alter the underlying editorial content or meaning of the Work used, and that the resulting material is used solely within the scope of, and in a manner consistent with, the particular License described in the Order Confirmation and the Terms.

15) **Miscellaneous.**

a) User acknowledges that CCC may, from time to time, make changes or additions to the Service or to the Terms, and that Rightsholder may make changes or additions to the Rightsholder Terms. Such updated Terms will replace the prior terms and conditions in the order workflow and shall be effective as to any subsequent Licenses but shall not apply to Licenses already granted and paid for under a prior set of terms.

b) Use of User-related information collected through the Service is governed by CCC's privacy policy, available online at www.copyright.com/about/privacy-policy/.

c) The License is personal to User. Therefore, User may not assign or transfer to any other person (whether a natural person or an organization of any kind) the License or any rights granted thereunder; provided, however, that, where applicable, User may assign such License in its entirety on written notice to CCC in the event of a transfer of all or substantially all of User's rights in any new material which includes the Work(s) licensed under this Service.

d) No amendment or waiver of any Terms is binding unless set forth in writing and signed by the appropriate parties, including, where applicable, the Rightsholder. The Rightsholder and CCC hereby object to any terms contained in any writing prepared by or on behalf of the User or its principals, employees, agents or affiliates and purporting to govern or otherwise relate to the License described in the Order Confirmation, which terms are in any way inconsistent with any Terms set forth in the Order Confirmation, and/or in CCC's standard operating procedures, whether such writing is prepared prior to, simultaneously with or subsequent to the Order Confirmation, and whether such writing appears on a copy of the Order Confirmation or in a separate instrument.

e) The License described in the Order Confirmation shall be governed by and construed under the law of the State of New York, USA, without regard to the principles thereof of conflicts of law. Any case, controversy, suit, action, or proceeding arising out of, in connection with, or related to such License shall be brought, at CCC's sole discretion, in any federal or state court located in the County of New York, State of New York, USA, or in any federal or state court whose geographical jurisdiction covers the location of the Rightsholder set forth in the Order Confirmation. The parties expressly submit to the personal jurisdiction and venue of each such federal or state court.

SPRINGER NATURE LICENSE TERMS AND CONDITIONS

Jul 14, 2022

This Agreement between Mr. Anton Lutsenko ("You") and Springer Nature ("Springer Nature") consists of your license details and the terms and conditions provided by Springer Nature and Copyright Clearance Center.

License Number	5320780914923
License date	Jun 02, 2022
Licensed Content Publisher	Springer Nature
Licensed Content Publication	Nature
Licensed Content Title	From quantum matter to high-temperature superconductivity in copper oxides
Licensed Content Author	B. Keimer et al
Licensed Content Date	Feb 11, 2015
Type of Use	Thesis/Dissertation
Requestor type	academic/university or research institute
Format	electronic
Portion	figures/tables/illustrations
Number of figures/tables /illustrations	1
High-res required	no
Will you be translating?	no
Circulation/distribution	1 - 29
Author of this Springer Nature content	no
Title	Modeling the X-ray absorption of Neodymium ions in cuprate superconductors
Institution name	University of Waterloo
Expected presentation date	Jul 2022
Portions	Figure 2: Phase diagram.
Requestor Location	Mr. Anton Lutsenko [redacted]
Total	**0.00 CAD**
Terms and Conditions	

Springer Nature Customer Service Centre GmbH
Terms and Conditions

This agreement sets out the terms and conditions of the licence (the **Licence**) between you and **Springer Nature Customer Service Centre GmbH** (the **Licensor**). By clicking 'accept' and completing the transaction for the material (**Licensed Material**), you also confirm your acceptance of these terms and conditions.

1. Grant of License

1. 1. The Licensor grants you a personal, non-exclusive, non-transferable, world-wide licence to reproduce the Licensed Material for the purpose specified in your order only. Licences are granted for the specific use requested in the order and for no other use, subject to the conditions below.

1. 2. The Licensor warrants that it has, to the best of its knowledge, the rights to license reuse of the Licensed

Material. However, you should ensure that the material you are requesting is original to the Licensor and does not carry the copyright of another entity (as credited in the published version).

1. 3. If the credit line on any part of the material you have requested indicates that it was reprinted or adapted with permission from another source, then you should also seek permission from that source to reuse the material.

2. Scope of Licence

2. 1. You may only use the Licensed Content in the manner and to the extent permitted by these Ts&Cs and any applicable laws.

2. 2. A separate licence may be required for any additional use of the Licensed Material, e.g. where a licence has been purchased for print only use, separate permission must be obtained for electronic re-use. Similarly, a licence is only valid in the language selected and does not apply for editions in other languages unless additional translation rights have been granted separately in the licence. Any content owned by third parties are expressly excluded from the licence.

2. 3. Similarly, rights for additional components such as custom editions and derivatives require additional permission and may be subject to an additional fee. Please apply to [redacted] for these rights.

2. 4. Where permission has been granted **free of charge** for material in print, permission may also be granted for any electronic version of that work, provided that the material is incidental to your work as a whole and that the electronic version is essentially equivalent to, or substitutes for, the print version.

2. 5. An alternative scope of licence may apply to signatories of the STM Permissions Guidelines, as amended from time to time.

3. Duration of Licence

3. 1. A licence for is valid from the date of purchase ('Licence Date') at the end of the relevant period in the below table:

Scope of Licence	**Duration of Licence**
Post on a website	12 months
Presentations	12 months
Books and journals	Lifetime of the edition in the language purchased

4. Acknowledgement

4. 1. The Licensor's permission must be acknowledged next to the Licenced Material in print. In electronic form, this acknowledgement must be visible at the same time as the figures/tables/illustrations or abstract, and must be hyperlinked to the journal/book's homepage. Our required acknowledgement format is in the Appendix below.

5. Restrictions on use

5. 1. Use of the Licensed Material may be permitted for incidental promotional use and minor editing privileges e.g. minor adaptations of single figures, changes of format, colour and/or style where the adaptation is credited as set out in Appendix 1 below. Any other changes including but not limited to, cropping, adapting, omitting material that affect the meaning, intention or moral rights of the author are strictly prohibited.

5. 2. You must not use any Licensed Material as part of any design or trademark.

5. 3. Licensed Material may be used in Open Access Publications (OAP) before publication by Springer Nature, but any Licensed Material must be removed from OAP sites prior to final publication.

6. Ownership of Rights

6. 1. Licensed Material remains the property of either Licensor or the relevant third party and any rights not explicitly granted herein are expressly reserved.

7. Warranty

IN NO EVENT SHALL LICENSOR BE LIABLE TO YOU OR ANY OTHER PARTY OR ANY OTHER PERSON OR FOR ANY SPECIAL, CONSEQUENTIAL, INCIDENTAL OR INDIRECT DAMAGES, HOWEVER CAUSED, ARISING OUT OF OR IN CONNECTION WITH THE DOWNLOADING, VIEWING OR USE OF THE MATERIALS REGARDLESS OF THE FORM OF ACTION, WHETHER FOR BREACH OF CONTRACT, BREACH OF WARRANTY, TORT, NEGLIGENCE, INFRINGEMENT OR OTHERWISE (INCLUDING, WITHOUT LIMITATION, DAMAGES BASED ON LOSS OF PROFITS, DATA, FILES, USE, BUSINESS OPPORTUNITY OR CLAIMS OF THIRD PARTIES), AND
WHETHER OR NOT THE PARTY HAS BEEN ADVISED OF THE POSSIBILITY OF SUCH DAMAGES. THIS LIMITATION SHALL APPLY NOTWITHSTANDING ANY FAILURE OF ESSENTIAL PURPOSE OF ANY LIMITED REMEDY PROVIDED HEREIN.

8. Limitations

8. 1. ***BOOKS ONLY:***Where **'reuse in a dissertation/thesis'** has been selected the following terms apply: Print rights of the final author's accepted manuscript (for clarity, NOT the published version) for up to 100 copies, electronic rights for use only on a personal website or institutional repository as defined by the Sherpa guideline (www.sherpa.ac.uk/romeo/).

8. 2. For content reuse requests that qualify for permission under the STM Permissions Guidelines, which may be updated from time to time, the STM Permissions Guidelines supersede the terms and conditions contained in this licence.

9. Termination and Cancellation

9. 1. Licences will expire after the period shown in Clause 3 (above).

9. 2. Licensee reserves the right to terminate the Licence in the event that payment is not received in full or if there has been a breach of this agreement by you.

Appendix 1 — Acknowledgements:

For Journal Content:
Reprinted by permission from [**the Licensor**]: [**Journal Publisher** (e.g. Nature/Springer/Palgrave)] [**JOURNAL NAME**] [**REFERENCE CITATION** (Article name, Author(s) Name), [**COPYRIGHT**] (year of publication)

For **Advance Online Publication papers:**
Reprinted by permission from [**the Licensor**]: [**Journal Publisher** (e.g. Nature/Springer/Palgrave)] [**JOURNAL NAME**] [**REFERENCE CITATION** (Article name, Author(s) Name), [**COPYRIGHT**] (year of publication), advance online publication, day month year (doi: 10.1038/sj.[JOURNAL ACRONYM].)

For Adaptations/Translations:
Adapted/Translated by permission from [**the Licensor**]: [**Journal Publisher** (e.g. Nature/Springer/Palgrave)] [**JOURNAL NAME**] [**REFERENCE CITATION** (Article name, Author(s) Name), [**COPYRIGHT**] (year of publication)

Note: For any republication from the British Journal of Cancer, the following credit line style applies:

Reprinted/adapted/translated by permission from [**the Licensor**]: on behalf of Cancer Research UK: : [**Journal Publisher** (e.g. Nature/Springer/Palgrave)] [**JOURNAL NAME**] [**REFERENCE CITATION** (Article name, Author(s) Name), [**COPYRIGHT]** (year of publication)

For **Advance Online Publication** papers:
Reprinted by permission from The [**the Licensor**]: on behalf of Cancer Research UK: [**Journal Publisher** (e.g. Nature/Springer/Palgrave)] [**JOURNAL NAME**] [**REFERENCE CITATION** (Article name, Author(s) Name), [**COPYRIGHT**] (year of publication), advance online publication, day month year (doi: 10.1038/sj.[JOURNAL ACRONYM])

For Book content:

American Physical Society
Reuse and Permissions License

02-Jun-2022

This license agreement between the American Physical Society ("APS") and Anton Lutsenko ("You") consists of your license details and the terms and conditions provided by the American Physical Society and SciPris.

Licensed Content Information

License Number:	**RNP/22/JUN/054357**
License date:	02-Jun-2022
DOI:	10.1103/PhysRevMaterials.4.114801
Title:	Materials preparation, single-crystal growth, and the phase diagram of the cuprate high-temperature superconductor $ {\mathrm{La}}_{1.6-x}{\mathrm{Nd}}_{0.4}{\mathrm{Sr}}_{x}\mathrm{Cu}{\mathrm{O}}_{4}$
Author:	Mirela Dragomir et al.
Publication:	Physical Review Materials
Publisher:	American Physical Society
Cost:	USD $ 0.00

Request Details

Does your reuse require significant modifications: No

Specify intended distribution locations:	Canada
Reuse Category:	Reuse in a thesis/dissertation
Requestor Type:	Student
Items for Reuse:	Figures/Tables
Number of Figure/Tables:	2
Figure/Tables Details:	Figure 1, Figure 14
Format for Reuse:	Electronic

Information about New Publication:

University/Publisher:	University of Waterloo
Title of dissertation/thesis:	Modeling the X-ray absorption of Neodymium ions in cuprate superconductors
Author(s):	Anton Lutsenko
Expected completion date:	Jul. 2022

License Requestor Information

Name:	Anton Lutsenko
Affiliation:	Individual
Email Id:	[redacted]
Country:	Canada

American Physical Society
Reuse and Permissions License

TERMS AND CONDITIONS

The American Physical Society (APS) is pleased to grant the Requestor of this license a non-exclusive, non-transferable permission, limited to Electronic format, provided all criteria outlined below are followed.

1. You must also obtain permission from at least one of the lead authors for each separate work, if you haven't done so already. The author's name and affiliation can be found on the first page of the published Article.
2. For electronic format permissions, Requestor agrees to provide a hyperlink from the reprinted APS material using the source material's DOI on the web page where the work appears. The hyperlink should use the standard DOI resolution URL, http://dx.doi.org/{DOI}. The hyperlink may be embedded in the copyright credit line.
3. For print format permissions, Requestor agrees to print the required copyright credit line on the first page where the material appears: "Reprinted (abstract/excerpt/figure) with permission from [(FULL REFERENCE CITATION) as follows: Author's Names, APS Journal Title, Volume Number, Page Number and Year of Publication.] Copyright (YEAR) by the American Physical Society."
4. Permission granted in this license is for a one-time use and does not include permission for any future editions, updates, databases, formats or other matters. Permission must be sought for any additional use.
5. Use of the material does not and must not imply any endorsement by APS.
6. APS does not imply, purport or intend to grant permission to reuse materials to which it does not hold copyright. It is the requestor's sole responsibility to ensure the licensed material is original to APS and does not contain the copyright of another entity, and that the copyright notice of the figure, photograph, cover or table does not indicate it was reprinted by APS with permission from another source.
7. The permission granted herein is personal to the Requestor for the use specified and is not transferable or assignable without express written permission of APS. This license may not be amended except in writing by APS.
8. You may not alter, edit or modify the material in any manner.
9. You may translate the materials only when translation rights have been granted.
10. APS is not responsible for any errors or omissions due to translation.
11. You may not use the material for promotional, sales, advertising or marketing purposes.
12. The foregoing license shall not take effect unless and until APS or its agent, Aptara, receives payment in full in accordance with Aptara Billing and Payment Terms and Conditions, which are incorporated herein by reference.
13. Should the terms of this license be violated at any time, APS or Aptara may revoke the license with no refund to you and seek relief to the fullest extent of the laws of the USA. Official written notice will be made using the contact information provided with the permission request. Failure to receive such notice will not nullify revocation of the permission.
14. APS reserves all rights not specifically granted herein.
15. This document, including the Aptara Billing and Payment Terms and Conditions, shall be the entire agreement between the parties relating to the subject matter hereof.

References

[1] J. Georg Bednorz and K. Alex Müller. Perovskite-type oxides—the new approach to high-T_c superconductivity. *Rev. Mod. Phys.*, 60:585–600, Jul 1988.

[2] B. Keimer, S. A. Kivelson, M. R. Norman, S. Uchida, and J. Zaanen. From quantum matter to high-temperature superconductivity in copper oxides. *Nature*, 518(7538):179–186, Feb 2015.

[3] A. J. Achkar, M. Zwiebler, Christopher McMahon, F. He, R. Sutarto, Isaiah Djianto, Zhihao Hao, Michel J. P. Gingras, M. Hücker, G. D. Gu, A. Revcolevschi, H. Zhang, Y.-J. Kim, J. Geck, and D. G. Hawthorn. Nematicity in stripe-ordered cuprates probed via resonant X-ray scattering. *Science*, 351(6273):576–578, 2016.

[4] Naman K. Gupta, Christopher McMahon, Ronny Sutarto, Tianyu Shi, Rantong Gong, Haofei I. Wei, Kyle M. Shen, Feizhou He, Qianli Ma, Mirela Dragomir, Bruce D. Gaulin, and David G. Hawthorn. Vanishing nematic order beyond the pseudogap phase in overdoped cuprate superconductors. *Proceedings of the National Academy of Sciences*, 118(34):e2106881118, 2021.

[5] N. Gupta and D. Hawthorn. Private communications (unpublished). 2021.

[6] D. J. Newman and Betty Ng. *Crystal Field Handbook*. Cambridge University Press, 2000.

[7] J. Mulak and Z. Gajek. *The effective crystal field potential*. Elsevier Science & Technology Books, 2000.

[8] Maurits W. Haverkort. Quanty for core level spectroscopy - excitons, resonances and band excitations in time and frequency domain. *Journal of Physics: Conference Series*, 712:012001, may 2016.

[9] M R Norman and C Pépin. The electronic nature of high temperature cuprate superconductors. *Reports on Progress in Physics*, 66(10):1547–1610, Sep 2003.

[10] J. G. Bednorz and K. A. Müller. Possible high-T_c superconductivity in the Ba-La-Cu-O system. *Zeitschrift für Physik B Condensed Matter*, 64(2):189–193, Jun 1986.

[11] M. K. Wu, J. R. Ashburn, C. J. Torng, P. H. Hor, R. L. Meng, L. Gao, Z. J. Huang, Y. Q. Wang, and C. W. Chu. Superconductivity at 93 K in a new mixed-phase Y-Ba-Cu-O compound system at ambient pressure. *Phys. Rev. Lett.*, 58:908–910, Mar 1987.

[12] R. J. Cava. Structural chemistry and the local charge picture of copper oxide superconductors. *Science*, 247(4943):656–662, 1990.

[13] Neven Barišić, Mun K. Chan, Yuan Li, Guichuan Yu, Xudong Zhao, Martin Dressel, Ana Smontara, and Martin Greven. Universal sheet resistance and revised phase diagram of the cuprate high-temperature superconductors. *Proceedings of the National Academy of Sciences*, 110(30):12235–12240, 2013.

[14] M. W. Shafer, T. Penney, and B. L. Olson. Correlation of T_c with hole concentration in $La_{2-x}Sr_xCuO_{4-\delta}$ superconductors. *Phys. Rev. B*, 36:4047–4050, Sep 1987.

[15] J. M. Tranquada, S. M. Heald, A. R. Moodenbaugh, G. Liang, and M. Croft. Nature of the charge carriers in electron-doped copper oxide superconductors. *Nature*, 337:720, February 1989.

[16] Mirela Dragomir, Qianli Ma, J. Patrick Clancy, Amirreza Ataei, Paul A. Dube, Sudarshan Sharma, Ashfia Huq, Hanna A. Dabkowska, Louis Taillefer, and Bruce D. Gaulin. Materials preparation, single-crystal growth, and the phase diagram of the cuprate high-temperature superconductor $La_{1.6-x}Nd_{0.4}Sr_xCuO_4$. *Phys. Rev. Materials*, 4:114801, Nov 2020.

[17] J. D. Axe and M. K. Crawford. Structural instabilities in lanthanum cuprate superconductors. *Journal of Low Temperature Physics*, 95:271–284, 1994.

[18] Louis Taillefer. Fermi surface reconstruction in high-T_c superconductors. *Journal of physics. Condensed matter : an Institute of Physics journal*, 21 16:164212, 2009.

[19] Heiko Wende. Recent advances in X-ray absorption spectroscopy. *Reports on Progress in Physics*, 67:2105–2181, 2004.

[20] Uwe Mueller, Ronald Förster, Michael Hellmig, Franziska U. Huschmann, Alexandra Kastner, Piotr Malecki, Sandra Pühringer, Martin Röwer, Karine Sparta, Michael Steffien, Monika Ühlein, Piotr Wilk, and Manfred S. Weiss. The macromolecular crystallography beamlines at BESSY II of the Helmholtz-Zentrum Berlin: Current status and perspectives. *The European Physical Journal Plus*, 130(7):141, Jul 2015.

[21] Pawel Grochulski, Michel N. Fodje, James Gorin, Shaunivan L. Labiuk, and Russ Berg. Beamline 08ID-1, the prime beamline of the Canadian Macromolecular Crystallography Facility. *Journal of Synchrotron Radiation*, 18(4):681–684, Jul 2011.

[22] M. W. Haverkort, N. Hollmann, I. P. Krug, and A. Tanaka. Symmetry analysis of magneto-optical effects: The case of x-ray diffraction and x-ray absorption at the transition metal $L_{2,3}$ edge. *Phys. Rev. B*, 82:094403, Sep 2010.

[23] K. Penc, J. Romhányi, T. Rõ om, U. Nagel, Á. Antal, T. Fehér, A. Jánossy, H. Engelkamp, H. Murakawa, Y. Tokura, D. Szaller, S. Bordács, and I. Kézsmárki. Spin-stretching modes in anisotropic magnets: Spin-wave excitations in the multiferroic $ba_2coge_2o_7$. *Phys. Rev. Lett.*, 108:257203, Jun 2012.

[24] Qing Tong and Shubo Wang. Acoustic helical dichroism in a one-dimensional lattice of chiral resonators. *Phys. Rev. B*, 105:024111, Jan 2022.

[25] M.T. Hutchings. *Point-charge calculations of energy levels of magnetic ions in crystalline electric fields*, volume 16 of *Solid State Physics*. Academic Press, 1964.

[26] Peter Fulde and Michael Loewenhaupt. Magnetic excitations in crystal-field split $4f$ systems. *Advances in Physics*, 34(5):589–661, 1985.

[27] E. Bauer and M. Rotter. *Magnetism of complex metal alloys: crystalline electric field effects*. World Scientific, 2009.

[28] M. Loewenhaupt. Crystal fields in low symmetry systems. *Physica B: Condensed Matter*, 163(1):479–482, 1990.

[29] David Borwein, Jonathan M. Borwein, and Keith F. Taylor. Convergence of lattice sums and Madelung's constant. *Journal of Mathematical Physics*, 26(11):2999–3009, 1985.

[30] Maurits W. Haverkort. XAS $L_{2,3}$ – Quanty documentation, 2018.

[31] Qianli Ma, Evan M. Smith, Zachary W. Cronkwright, Mirela Dragomir, Gabrielle Mitchell, Alexander I. Kolesnikov, Matthew B. Stone, and Bruce D. Gaulin. Dynamic parallel spin stripes from the 1/8 anomaly to the end of superconductivity in $La_{1.6-x}Nd_{0.4}Sr_xCuO_4$. *Phys. Rev. Research*, 4:013175, Mar 2022.

[32] G. Riou, S. Jandl, M. Poirier, V. Nekvasil, M. Maryško, J. Fábry, K. Jurek, M. Diviš, J. Hölsä, I. M. Sutjahja, A. A. Menovsky, S. N. Barilo, S. V. Shiryaev, and L. N. Kurnevich. Infrared transmission study of crystal-field excitations in $La_{1.6-x}Nd_{0.4}Sr_xCuO_4$. *Phys. Rev. B*, 66:224508, Dec 2002.

[33] J. Fink, N. Nücker, E. Pellegrin, H. Romberg, M. Alexander, and M. Knupfer. Electron energy-loss and X-ray absorption spectroscopy of cuprate superconductors and related compounds. *Journal of Electron Spectroscopy and Related Phenomena*, 66(3):395–452, 1994.

[34] A.J. Freeman and J.P. Desclaux. Dirac-Fock studies of some electronic properties of rare-earth ions. *Journal of Magnetism and Magnetic Materials*, 12(1):11–21, 1979.

[35] Marius Retegan. Crispy: v0.7.3, 2019.

APPENDICES

Appendix A

Tools and methods

The work was carried via Lua script files, which were initially based on the file produced by Crispy (Ref. [35]) but reworked and repurposed. The spectra calculation script consists of several parts:

1. Calculation variables definition

   Each spectrum was produced on the range from 970.4 to 1000.4 eV, having 2000 points on this interval. For calculating the Green function, Lorentzian FWHM Γ = 0.1 eV was used, and each calculated spectrum was broadened further, with total Lorentzian FWHM of 0.96 eV.

2. Model configuration variables

   This includes Boolean variables to enable or disable specific terms of the Hamiltonian:

   - `AtomicTerm` (Coulomb potential, kinetic energy, and Coulomb repulsion),
   - `CrystalFieldTerm4f`,
   - `LigandHybridizationTerm`,
   - `MagneticFieldTerm`, and
   - `ExchangeFieldTerm`.

Incoming ray wave vector was chosen to be in Ox direction, while horizontal polarization corresponded to Oy, and vertical – to Oz;

3. Functions definitions

   Some of the main functions declared in this scope are:

   - `WavefunctionsAndBoltzmannFactors()` – used to calculate eigenstates for a given Hamiltonian, as well as corresponding eigenenergies and Boltzmann factors for a given temperature;
   - `GetSpectrum()` – used to obtain a thermal average of the spectra, corresponding to different initial energy states;
   - `SaveSpectrum()` – used to broaden the spectrum and print it to a file for further analysis.

4. Hamiltonian assembly, analysis and spectra production

   The Nd^{3+} ion was modeled as two electron shells: fully occupied 3d core shell and a valence shell having 3 electrons. Each of the $5 + 7 = 12$ orbitals could have a spin-up and/or a spin-down electron, making in total 24 available modes. Next, initial Hamiltonian (before the X-ray impact, with $3d^{10}4f^3$ configuration) and final Hamiltonian (after the impact, with $3d^9 4f^4$ configuration) are constructed by adding respective terms. After the assembly, the eigenstates are calculated from the initial Hamiltonian. They are used to calculate the Green functions for the final Hamiltonian with transition operators, corresponding to vertical and horizontal polarization of the incoming X-rays.

5. Temperature scaling

   Each of the eigenstates produces a specific absorption spectrum. The electron occupation of the eigenstates follows the Boltzmann distribution:

   $$p \propto e^{-\frac{E-E_g}{kT}}$$

   Consequently, the resulting absorption profile is a weighted sum of the absorption profiles of all the eigenstates, scaled by a corresponding Boltzmann factor. At this

step, Boltzmann factors are calculated for a given list of temperatures, and the corresponding spectra are produced and saved to text files.

6. envelope loop for producing the spectra for different values of given parameters. The steps above produce a set of spectra for a particular set of parameters (e.g. CEF parameters, magnetic field etc.). If multiple values of a parameter need to be checked, the `for` loop is used to iterate over a list of parameter values.

Appendix B

Crystal field parameter correlation diagrams

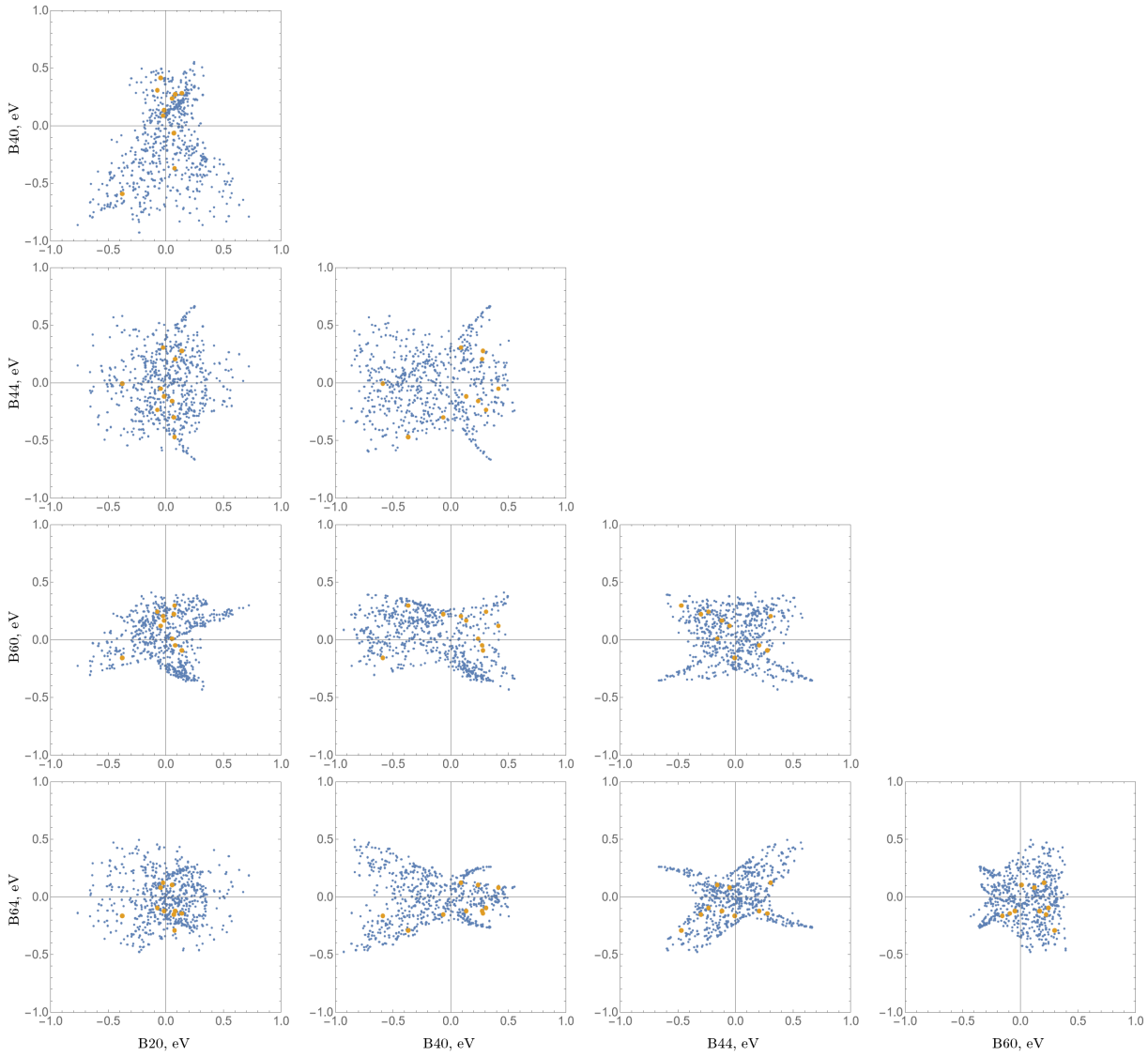

Figure B.1: Correlation diagram for Wybourne $B_{k,q}$ parameters. x-axis is the same for each column, and corresponds to (from left to right): $B_{2,0}$, $B_{4,0}$, $B_{4,4}$, $B_{6,0}$. y-axis is the same for each row, and corresponds to (from top to bottom): $B_{4,0}$, $B_{4,4}$, $B_{6,0}$, $B_{6,4}$. Blue dots represent the parameter sets which have Euclidean distance from the desired 11, 25, 45 energies less than 5 meV. Yellow dots correspond to the points which have the spectrum matching the criteria for experimental spectrum.

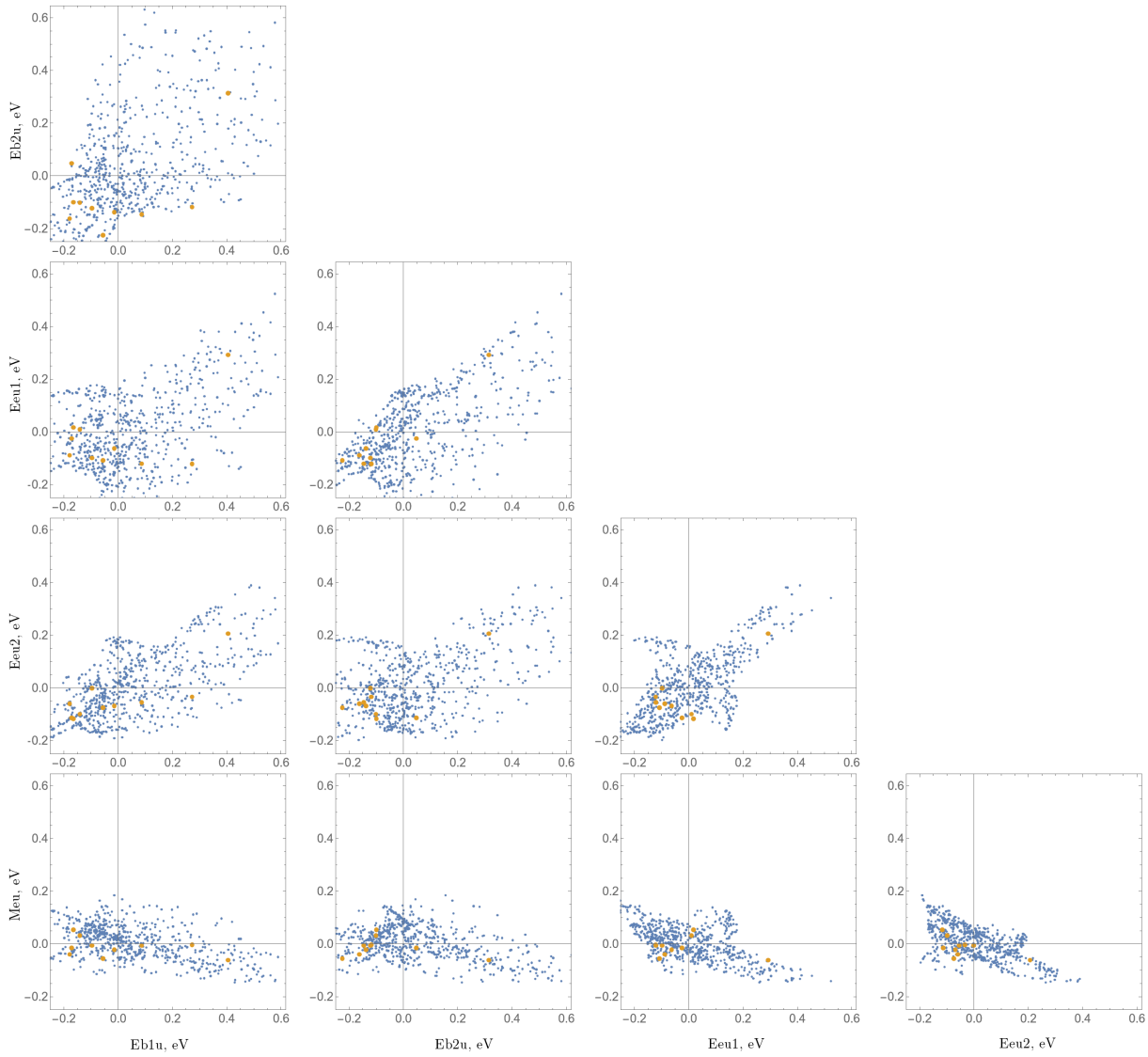

Figure B.2: Correlation diagram for one-electron energies. x-axis is the same for each column, and corresponds to (from left to right): E_{b1u}, E_{b2u}, E_{eu1}, E_{eu2}. y-axis is the same for each row, and corresponds to (from top to bottom): E_{b2u}, E_{eu1}, E_{eu2}, M_{eu}. Blue dots represent the parameter sets which have Euclidean distance from the desired 11, 25, 45 energies less than 5 meV. Yellow dots correspond to the points which have the spectrum matching the criteria for experimental spectrum.